JPhys Materials

PURPOSE-LED PUBLISHING™

TOPICAL REVIEW • OPEN ACCESS

Near-infrared-detectable artificial synapses for advanced neuromorphic vision applications

To cite this article: Minjun Choi *et al* 2025 *J. Phys. Mater.* **8** 042001

Journal of Physics: Materials

TOPICAL REVIEW

Near-infrared-detectable artificial synapses for advanced neuromorphic vision applications

Minjun Choi[1,5], Gwoncheol Choi[1,5], Seungbeom Lee[1], Tae-Woo Lee[2,3,4,*] and Hea-Lim Park[1,*]

[1] Department of Materials Science and Engineering, Seoul National University of Science and Technology, Seoul 01811, Republic of Korea
[2] Department of Materials Science and Engineering, Seoul National University, Seoul 08826, Republic of Korea
[3] Institute of Engineering Research, Research Institute of Advanced Materials, Soft Foundry, Interdisciplinary Program in Bioengineering, Seoul National University, Seoul 08826, Republic of Korea
[4] SN Display Co., Ltd., Seoul 08826, Republic of Korea
[5] These authors contributed equally to this work.
[*] Authors to whom any correspondence should be addressed.

E-mail: twlees@snu.ac.kr and parkhl21@seoultech.ac.kr

Keywords: near-infrared, artificial synapse, night vision, robotic control, motion recognition system

OPEN ACCESS

RECEIVED
26 February 2025

REVISED
19 May 2025

ACCEPTED FOR PUBLICATION
23 July 2025

PUBLISHED
31 July 2025

Abstract

The integration of near-infrared (NIR) light detection with artificial synaptic devices holds immense potential for advancing neuromorphic vision systems, enabling energy-efficient and high-speed data processing beyond conventional von Neumann architectures. NIR wavelengths provide critical information that visible light cannot offer owing to its high permeability and low scattering properties. This capability is particularly valuable for night vision, biomedical imaging, and autonomous sensing applications. However, existing artificial visual systems face challenges such as data transfer bottlenecks and high energy consumption, due to the separation of sensors and processors, as well as the need for digital conversion processes. NIR-responsive artificial synapses address these limitations by integrating NIR optical detection with synaptic computation, mimicking biological neural processing to achieve real-time data integration and adaptive learning. This review provides a comprehensive overview of recent advancements in NIR-detectable artificial synapses. We begin by discussing the fundamental biological synaptic properties essential for artificial synapse operation. Next, we explore the NIR-responsive materials employed in artificial synapses and the principles enabling their synaptic properties, with particular attention to device architectures. Additionally, we examine two practical applications including night vision systems and robotic control systems. Finally, we address the remaining challenges facing the field and propose future research directions for the development of this promising technology.

1. Introduction

Near-infrared light (NIR), with a wavelength range of 750 nm to 2.5 μm, is distinct from visible light [1]. It provides complementary and enriched information beyond what visible light can offer. Due to its high transmittance, NIR can penetrate deeper beneath the surface than visible light, making it particularly useful for applications such as non-destructive testing and medical diagnostics [2–6]. Additionally, its longer wavelength results in reduced scattering, allowing for more stable imaging under challenging conditions such as fog. As a result, NIR delivers clearer images with better contrast and less noise [7]. These advantages make it valuable for wireless remote control systems and as a complement to visible light imaging in applications requiring robust and stable imaging, such as autonomous vehicles [8, 9]. Moreover, NIR is widely used for exclusive visibility in low-light environments, including security and minimal night vision applications [9–11]. Unlike thermal imaging, which captures temperature variations using mid- to long-wave infrared radiation (above 2.5 μm) emitted by objects, NIR imaging detects reflected light, producing images that closely resemble visual perception. This allows for clearer object outlines and pattern recognition, making NIR images compatible with visible light image processing [12, 13].

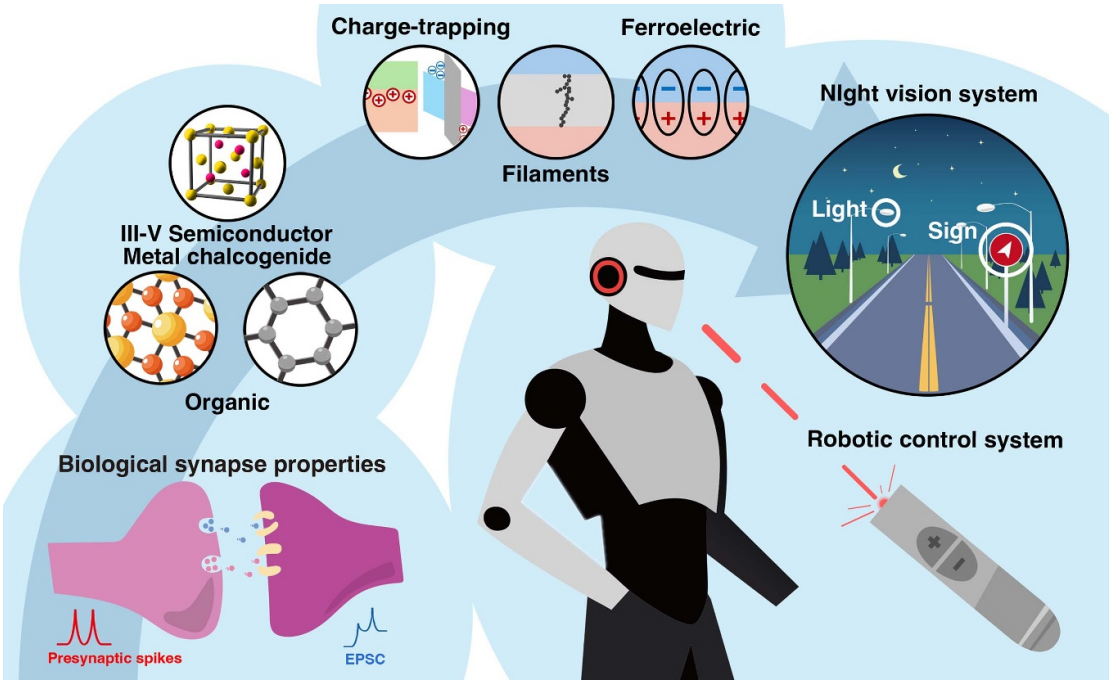

Figure 1. A schematic illustrating biological synaptic properties, materials for NIR light detection, underlying mechanisms for implementing NIR-detectable artificial synapses, and key applications utilizing NIR properties.

However, such applications generate vast amounts of data owing to high pixel densities and high sampling rates, which leads bottleneck in conventional von Neumann architecture. These limitations result from seperation between memory and processing units, which leads to slower processing and increased energy consumption [14]. Therefore, neuromorphic computing, which emulates the information processing methods of the biological brain, has been introduced as an alternative to von Neumann architectures to efficiently process the data [15–17]. Compared to von Neumann architecture, biological neural networks process and store information simultaneously by dynamically adjusting the weights of interconnected synapses, enabling rapid and efficient handling of large data volumes. Furthermore, in the human brain, each neuron communicates with others via spikes, and synapses learn by adjusting their weights in response to these spike signals. To emulate such spiking neural network systems, artificial synapses that mimic the properties of biological synapses must be developed, which could be a step toward realizing neuromorphic computing that more closely resembles the biological brain [18–23].

Biological vision systems have evolved to process diverse visual information with remarkable speed, efficiency, and accuracy, offering pivotal inspiration for the design of artificial vision systems [24]. Emulating the underlying processing mechanisms and specialized anatomical architectures of natural visual systems—such as parallel information processing and features like the compound eyes and curved retinas of insects and crustaceans—represents a key strategy in the development of next-generation artificial vision technologies [25]. Artificial synapses play a crucial role in enabling such biologically inspired systems. Their intrinsic capabilities for parallel and spiking-based signal processing allow for efficient, real-time handling of complex visual stimuli. Moreover, exploiting the synaptic divergence of artificial synaptic devices facilitates simultaneous processing of heterogeneous sensory inputs. By tailoring device characteristics and optimizing array-level architectures, it becomes feasible to mimic the aforementioned physical features, thereby enhancing the performance and functional adaptability of artificial vision platforms.

Recently, researchers have developed artificial synapses capable of detecting NIR [26, 27] (figure 1). These NIR-detectable artificial synapses emulate the functions of photoreceptor cells and neurons in the biological eye and brain, drawing inspiration from biological neural networks. In these devices, NIR signals are transmitted to optical artificial synapses, where synaptic plasticity is regulated to enable simultaneous data storage and information processing. This facilitates efficient applications such as complex image recognition and wireless remote control systems.

In this review, we examine recent advancements in NIR-detectable artificial synapses. We begin by discussing the biological principles underlying synaptic behavior and how they are emulated in these devices. We then explore the materials enabling NIR detection and the operating mechanisms of NIR-detectable artificial synapses. Next, we highlight their practical applications, including night vision and robotic control

systems. Finally, we address the current challenges in the field and propose future research directions for the development of this emerging technology.

2. Synaptic properties

2.1. Operation and characteristics of biological synapses

The human brain consists of neurons and synapses that interconnect them. Synapses can be classified into electrical and chemical types, each transmitting signals through different mechanisms. Electrical synapses facilitate rapid, bidirectional signal transmission via gap junctions [28, 29]. In contrast, chemical synapses rely on interactions among receptors, ions, ion channels, and neurotransmitters to transmit signals. This process generates post-synaptic potentials (PSPs) at the post-synaptic membrane. When the pre-synaptic membrane potential surpasses a certain threshold, an action potential is initiated and propagates along the axon to the terminal. Upon reaching the pre-synaptic membrane, the action potential triggers the opening of Ca^{2+} ion channels, allowing calcium ions to enter. This influx induces the release of neurotransmitters into the synaptic cleft (figure 2(a)). These neurotransmitters then bind to specific receptors based on their types [30–34]. At excitatory synapses, neurotransmitters primarily bind to ionotropic glutamate receptors on the post-synaptic membrane, opening cation channels (Na^+, K^+, and Ca^{2+}). The influx of cations depolarizes the PSP, shifting it in a positive direction—a process known as excitatory PSP [34]. Conversely, in inhibitory synapses, neurotransmitters interact with receptors (mainly ionotropic γ-aminobutyric acid (GABA-A) receptors) and activate the Cl^- ion channels. The influx of Cl^- ions leads to hyperpolarization, shifting the PSP in a negative direction, resulting in inhibitory PSP [31]. PSPs can be integrated through spatial or temporal summation (figure 2(b)). Spatial summation occurs when multiple pre-synaptic inputs combine, while temporal summation integrates PSPs from a single pre-synaptic neuron subjected to repeated stimulation. If the integrated PSP reaches the threshold, an action potential is generated and propagated to the next synapse.

Synaptic strength is dynamically modulated by synaptic activity, a phenomenon known as synaptic plasticity. This plasticity is broadly categorized into short-term and long-term plasticity, each further divided into potentiation and depression. In short-term plasticity, changes in PSPs—such as short-term potentiation (STP) and short-term depression (STD)—are transient, typically reverting to baseline within milliseconds. These effects are commonly observed as paired-pulse facilitation (PPF) and paired-pulse depression (PPD), respectively (figure 2(c)) [35, 36]. In PPF, consecutive stimulations lead to an increased release of neurotransmitters, enhancing PSP amplitudes at the post-synapse. In contrast, PPD occurs when receptor availability decreases due to weak or infrequent action potentials, leading to reduced PSP amplitudes. PPF and PPD are quantitatively expressed as follows [37, 38]:

$$\text{PPF (PPD) index} = \frac{A_2}{A_1} \times 100\,(\%)$$

where A_1 and A_2 represent the peak amplitudes of the first and second stimulations, respectively. The PPF index increases as the interval between consecutive stimulations decreases, while the PPD index exhibits the opposite trend.

Short-term plasticity can transition into long-term potentiation (LTP) or long-term depression (LTD) through persistent stimulation [39, 40] (figure 2(d)). In LTP, repeated stimulation strengthens synaptic connections, whereas in LTD, weak or infrequent stimuli weaken synaptic strength. These long-lasting changes can persist from minutes to months. The transition between different forms of plasticity is influenced by stimulus timing and frequency. Spike timing-dependent plasticity (STDP) describes how synaptic strength is modulated based on the time interval ($\Delta t = t_{post} - t_{pre}$,) between pre- and post-synaptic spikes, forming the basis of Hebbian learning. By varying Δt, different STDP patterns—such as Hebbian, anti-Hebbian, symmetrical, and visual STDP—can emerge [41–44]. Similarly, spike rate-dependent plasticity (SRDP) describes how synaptic weight is adjusted based on the frequency of pre- and post-synaptic spikes. These mechanisms are fundamental to information processing, memory, and learning in the brain.

2.2. Emulation of synaptic behavior

To replicate biological processes of synapses, artificial synapses have been designed to emulate key synaptic properties such as short-term and long-term plasticity, PPF/PPD, STDP, and SRDP using electrical or optical stimuli [45–48]. Considering these characteristics, artificial synapses are typically evaluated with the following parameters such as energy consumption, response time, retention time, and fault tolerance to assess their fidelity to biological systems. These parameters and the emulated synaptic properties of NIR-detectable artificial synapses are summarized in table 1.

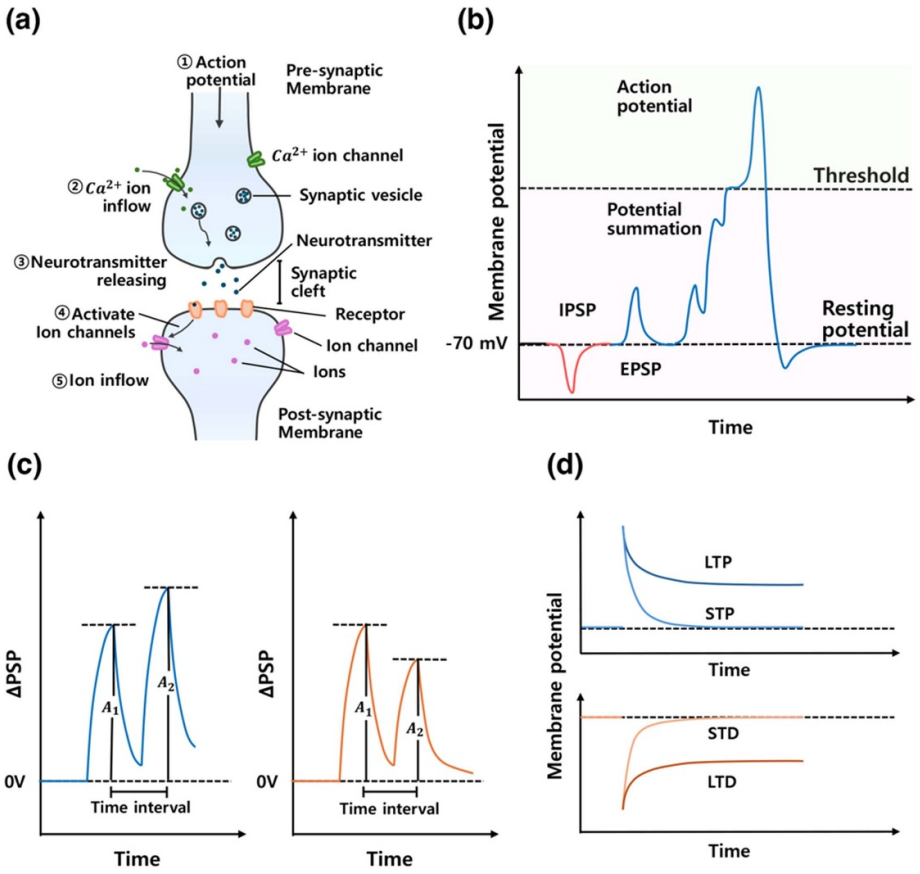

Figure 2. Schematic representation of various synaptic properties. (a) Structure and signal transmission process of chemical synapses, along with their components. (b) Graphs depicting membrane potential changes in postsynaptic potentials, including inhibitory and excitatory PSPs and potential summation, upon stimulation. (c) Graphs illustrating PPF (left) and PPD (right) in response to two consecutive signals received with a time interval. (d) Graphs showing long-term and short-term plasticity in potentiation (top) and depression (bottom).

In optoelectronic synapses, post-synaptic current (PSC) can be modulated by both electrical and optical signals, analogous to PSPs in biological synapses. These emulated devices achieved comparable or even lower energy consumption than biological synapses, typically in the range of 1–10 fJ [37]. Especially, a device employing elastomer styrene-ethylene-butylene-styrene and perovskite dots of $CsPbBr_3$ exhibited the energy consumption per spike of 15 aJ at the light with 6.41 μW cm^{-2} [61]. Meanwhile, the fast response time of optoelectronic synapses enables the *in-situ* image processing as the biological retina, and this property has been studied to be similar or faster. The synaptic device utilizing $MoSe_2$/MoTe achieved a response time of 188 μs, which is lower than the photoresponse of a few milliseconds in biological photoreceptors [56, 62]. In addition, PPF is emulated in general for synaptic devices, as it constitutes a fundamental feature of short-term plasticity [50, 56, 57, 63]. Synaptic weight modulation from short-term plasticity to long-term plasticity can be achieved additionally by controlling pulse duration or frequency, giving rise to spike duration-dependent plasticity (SDDP) and SRDP, respectively. For instance, the artificial synapse employing $MoSe_2$ superlattice as an NIR-photoresponsive material achieved the retention time above 100 s by SDDP, compared to milliseconds of biological synapses [50]. High fault tolerance has been achieved in artificial neural networks (ANNs) composed of optoelectronic synaptic devices. The fault tolerance of the devices can be evaluated by analyzing classification accuracy of ANN under induced noise—which demonstrates normal operation of the devices despite inter-ference from the noise of input signals. The fault tolerance of ANNs can be evaluated by analyzing classification accuracy under induced noise. Notably, an ANN based on NIR-detectable artificial synapses using Te/Bi_2Se_3 reached accuracy of 89.9% under a noise level of 70% [54].

3. Implementation of NIR-detectable artificial synapses

In order to implement NIR-detectable artificial synapses, devices should meet two key requirements. First, it is required to include a photoresponsive layer capable of detecting NIR light. Since NIR light has a wavelength range of 750–2500 nm, the materials used for the photoresponsive layer should have a low

Table 1. Summary of synaptic properties and device characteristics of NIR-detectable artificial synapses.

Device structure	Photosensitive material	Retention time	Synaptic properties	Energy consumption[a]	Response time	Accuracy	References
Two-terminal	PbS QDs	—	STP/STD, PPF, LTP/LTD, SRDP, SNDP	$E_{tot} = 65$ nJ[a] ($V = 0.01$ V)	—	81.9% (ANN) (noise level = 60%)	[49]
	$MoSe_2$ superlattice	>100 s	STP, PPF, LTP, SDDP, SNDP	$E_{elec} = 10$ fJ ($V = 0.1$ V)	—	—	[50]
	IEICO-4F	>4500 s	STP, PPF, LTP, SDDP, SNDP	$E_{tot} = 112$ nJ ($V = 0.65$ V)	—	—	[51]
	$MoSe_2/Bi_2Se_3$	$>10^6$ s	STP/STD, PPF/PPD, LTP/LTD, SRDP	$E_{elec} = 100$ nJ ($V = 0.5$ V)	—	—	[52]
	O_D-IGZO/O_R-IGZO	$>10^4$ s	LTP/LTD, STDP	—	—	—	[53]
Three-terminal	Te/Bi_2Se_3	—	LTP/LTD	—	—	89.9% (ANN) (noise level = 70%)	[54]
	Si-rich SiN_x	>1000 s	LTP/LTD	—	8 ms	~ 85% (CNN) ($\sigma^b = 1.75$)	[55]
	$MoS_2/MoTe_2$	>1 h	STP, PPF, LTP/LTD, SRDP	—	188 μs	>60% (noise level = 20%)	[56]
	P(gNDI-gT2)	>100 s	PPF, LTP/LTD	—	—	74.88% (ANN) ($\sigma = 0.2$)	[57]
	$CuInSe_2$ QDs	>1000 s	STP, PPF/PPD, LTP/LTD, SRDP, SNDP	$E_{elec} = 75$ aJ ($V_{ds} = -0.1$ mV)	—	45% (ANN) (noise level = 30%)	[58]
	$SnSe_2/WSe_2$	—	STP, LTP	—	2 ms	—	[59]
	COTIC-4F	—	STD, LTP/LTD, SDDP, SNDP	—	30 ms	54.0% (ANN) (noise level = 40%)	[60]

E_{tot} = Total power consumption per spike; E_{elec} = Electrical power consumption per spike; ANN = Artificial neural network; CNN = Convolutional neural network.

[a] This value was calculated by adding electrical and optical energy consumption, that is, using the formula of $V \times I \times t + S \times P_{in} \times t$ (V: applied voltage in device, I: current changes in optical pulse, S: photoresponsive layer area, P_{in}: light power, t: pulse duration time) [51].

[b] σ represents the standard deviation of the Gaussian noise in MNIST.

bandgap of 1.55 eV or less. Second, the device should exhibit synaptic behavior when exposed to NIR light. This synaptic behavior arises from the structural design of the device and the intrinsic properties of the materials used. In this chapter, we discuss the materials employed as NIR-photoresponsive layers and explore the mechanisms underlying the implementation of NIR-detectable artificial synapses.

3.1. Materials

To detect the NIR light, III–V compound semiconductors, metal chalcogenides, and organic materials have been widely utilized. The properties and comparison of the devices that utilize these materials are summarized in table 2. In this section, we review these materials, their properties, and studies that have applied them to artificial synapses.

3.1.1. III-V semiconductors

III–V compound semiconductors are composed of Group III elements (e.g. Al, Ga, In) and Group V elements (e.g. N, P, As, Sb) and are well known for their high carrier mobility [73]. Among these, materials such as InP, InN, and GaAs exhibit a narrow bandgap, making them suitable for NIR light detection. As a result, they have been widely used as photoresponsive layers in NIR detectors [74, 75]. III–V compound semiconductors are primarily synthesized using chemical vapor deposition or molecular beam epitaxy (MBE). Additionally, ternary and quaternary compounds, such as InGaSb and InGaAsP, enable bandgap tuning by adjusting their stoichiometric ratios during synthesis. For instance, $In_{0.53}Ga_{0.47}As$, with a low bandgap of 0.75 eV, has demonstrated a photoresponse under illumination with a 1550 nm wavelength in artificial synapses [64]. However, many III–V semiconductors are typically used at low temperatures (below 100 K) due to the degradation of NIR detection performance at room temperature, which is caused by increased dark current from carrier generation-recombination processes and minority carrier diffusion [76–79]. To mitigate this issue, nanowire structures have been introduced. Their large surface-to-volume ratio minimizes active volume, reducing dark current (figure 3(a)). Additionally, nanowires have a rich surface state that enhances carrier lifetime, while their low-dimensional structure facilitates efficient carrier transport. As a result, nanowires exhibit high photoconductive gain and improved light sensitivity [74, 75]. These properties make III–V compound semiconductors well suited for photosensitive applications, such as image recognition in artificial synapses. For instance, InAs, which has a low bandgap of ∼0.35 eV, has been utilized at low temperatures (down to 77 K) to achieve efficient performance. To enhance photoresponse to NIR light at room temperature, InAs has been utilized in nanowire structures, which enhance electron mobility and light absorption. This approach reduced dark current to just a few nA at room temperature while demonstrating photoresponse across the NIR spectrum (750–1550 nm) in artificial synapses [65]. Similarly, InN, with a low bandgap of 0.6 eV, has been explored in nanowire structures for NIR photodetector applications. InN nanowires have exhibited high photoconductivity at room temperature [80]. For example, InN nanowires showed a photoresponse under 808 nm illumination, highlighting their potential for NIR-detectable artificial synapses.

3.1.2. Metal chalcogenides

Metal chalcogenides, composed of metal elements (e.g. In, Pb, Bi, Cd, Mo) and chalcogen anions (e.g. S, Se, Te), exhibit varying bandgaps depending on their composition and crystal structure [82, 83]. Their ability to absorb light at specific wavelengths makes them highly attractive for light detection applications. Metal chalcogenides are commonly used in low-dimensional structures, such as quantum dots (QDs) and two-dimensional (2D) materials. In the case of QDs, they can be synthesized through various deposition methods such as colloidal synthesis and chemical vapor deposition, while 2D metal chalcogenides can be created typically by atomic layer deposition and mechanical/chemical/liquid-phase exfoliation [84–87]. These materials enhance light absorption and optoelectronic performance due to their large surface-to-volume ratio [88–90]. Low-bandgap metal chalcogenides, such as PbS, $CuInSe_2$, and $MoSe_2$, have been incorporated into QDs and 2D materials for NIR-detectable artificial synapses.

QDs are zero-dimensional materials with nanometer-scale sizes that exhibit unique optical properties due to the quantum confinement effect [91–94]. This effect enables bandgap modulation by adjusting QD core size—larger QDs exhibit a reduced bandgap, allowing them to detect longer wavelengths (figure 3(b)) [95–97]. For example, PbS QDs that are widely used as NIR-photosensitive layers in artificial synapses exhibited bandgaps of 0.78 eV and 0.9 eV with diameters of 6 nm and 5 nm, respectively, with larger QDs detecting longer wavelengths [63, 68]. In addition, metal chalcogenides with ternary compounds have also been employed with QD structure. For instance, $CuInSe_2$ QDs, with an average diameter of 10 nm and a bandgap of 1.2 eV, have demonstrated a photoresponse at 850 nm in the NIR region [58]. Furthermore, ligand engineering is available to consider for enhancing QDs performance. Certain ligands can narrow the bandgap by aligning the energy levels between the highest occupied molecular orbital (HOMO) of the ligand

Table 2. Summary of material properties according to their types.

Material types	Photosensitive material	Dimension	Thermal stability[a]	Scalability	Bandgap (eV)	Responsivity (R) (A/W)	References
III–V semiconductors	InGaAs	3D	Low[b]	Low	0.75	1.74×10^6 (1550 nm)	[64]
	InAs	1D	Moderate[c]	Moderate	0.35	839.3 (750 nm)	[65]
Metal chalcogenides	$MoSe_2$ superlattice	2D	High	Moderate	—	—	[50]
	$SnSe_2/WSe_2$				0.1 (staggered)	5.5 (1600 nm)	[59]
	In_2Se_3/MoS_2				0.1 (staggered)	—	[66]
	$MoSe_2/Bi_2Se_3$				—	—	[52]
	WSe_2/In_2Se_3				—	—	[67]
	PbS QDs	0D	High	High	0.9	—	[63]
	PbS QDs				0.78	1.90×10^2 (1550 nm)	[68]
	$CuInSe_2$ QDs				1.2	0.5×10^{-2}	[58]
Organic materials	IEICO-4F	—	High	High	1.25	0.43 (880 nm)	[51]
	COTIC-4F				1.1	$>10^5$ (850–1064 nm)	[60]
	Y6				1.33	200 (808 nm)	[69]
	P1				0.69	$>5 \times 10^{-5}$ (1750 nm)	[37]
	PDPPBTT				—	—	[70]
	PBTT				—	—	[71]
	29SVS				—	—	[72]

29SVS = poly [2,5-bis(7-decylnonadecyl) pyrrolo [3,4-c]pyrrole-1,4(2H,5H)-dione-(E)-1,2-bis(5-(thiophen-2-yl) selenophen-2-yl)ethene].

[a] Thermal stability represents the stability of a material in detecting NIR light at room temperature.

[b] 3D III–V semiconductor suffers the performance degradation from dark current at room temperature.

[c] 1D III–V semiconductor reduces the dark current by forming a nanowire structure.

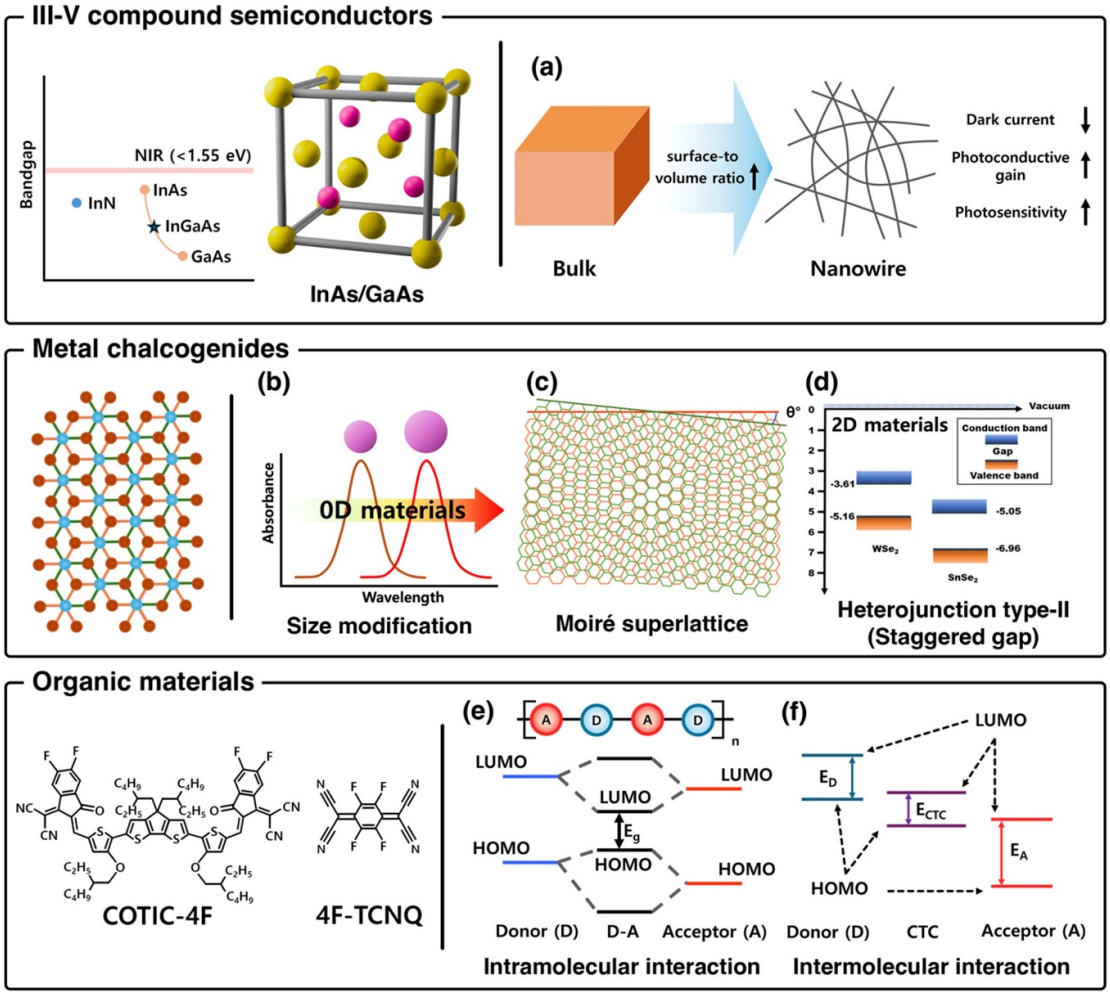

Figure 3. Photoresponsive materials used in artificial synapses and their strategies to detect NIR light. (a) Strategy for III–V compound semiconductors to reduce dark current while enhancing photoconductive gain and photosensitivity using nanowire structures, which possess a relatively higher surface-to-volume ratio compared to bulk structures. (b)–(d) Strategies for metal chalcogenides with QDs and 2D structure. (b) Wavelength shift in the absorption spectra of metal chalcogenide QDs as a function of increasing particle size. (c) Moiré patterns in 2D metal chalcogenides formed by stacking monolayers at specific twist angles [81]. (d) Energy band diagram illustrating the formation of a type-II heterojunction in 2D metal chalcogenides with staggered bandgap, specifically WSe_2 and $SnSe_2$. Reproduced from [59]. © IOP Publishing Ltd All rights reserved. (e), (f) Strategies for organic materials to reduce bandgap. (e) Bandgap reduction in organic materials achieved through donor–acceptor (D–A) structures, where intramolecular charge transfer creates new highest occupied molecular orbital (HOMO) and lowest unoccupied molecular orbital (LUMO) levels through interaction between donor and acceptor units. (f) Bandgap reduction via intermolecular interactions between organic donor and acceptor materials, forming charge transfer complexes (CTCs) with orbital hybridization and overlap.

and the valence band edge of the QD [98, 99]. For instance, tetrabutylammonium iodide (TBAI) has been used as a ligand for PbS QDs because it exhibits a red-shifted light absorption spectrum compared to oleic acid, which is commonly used as a ligand. Similarly, 1,2-ethanedithiol (EDT) has also been employed as a ligand for PbS QDs, demonstrating that while the bandgap reduction of PbS QDs with EDT is comparable to that with TBAI, light absorption in the NIR region is significantly enhanced with EDT [49, 100]. This study suggests that the combination of QDs and ligands can enhance both light absorption and bandgap reduction.

2D materials can be vertically stacked via van der Waals (vdW) forces, forming moiré superlattices through controlled twisting between layers (figure 3(c)). These periodic moiré patterns lead to bandgap narrowing, enabling long-wavelength NIR detection [81, 101–104]. For example, a $MoSe_2$ moiré superlattice detected wavelengths up to 1700 nm when twisted to a 30° angle, whereas a $MoSe_2$ monolayer exhibited no photoresponse at 1060 nm [50]. These findings demonstrate the potential of moiré superlattices for enabling long-wavelength NIR detection. Additionally, 2D materials can form heterostructures by stacking multiple layers. Unlike conventional materials, 2D heterostructures are free from lattice mismatch constraints due to their in-plane covalent bonding and absence of dangling bonds [89]. Heterostructures enable NIR detection through energy band alignment, particularly type-II (staggered) alignment, which facilitates carrier separation at the interface and reduces the effective bandgap, enabling NIR light detection [105–108]. For

instance, $WSe_2/SnSe_2$ heterostructures exhibited a photoresponse at 1600 nm, despite WSe_2 (bandgap: 1.90 eV) and $SnSe_2$ (bandgap: 1.51 eV) individually lacking NIR sensitivity. The heterostructure reduced the bandgap to 0.1 eV (figure 3(d)) [59]. Similarly, heterostructures composed of In_2Se_3 and MoS_2 exhibited a reduced optical bandgap of 0.1 eV, compared to their individual bandgaps of 0.74 and 1.68 eV, respectively [66].

3.1.3. Organic materials

Organic materials for NIR light detection in artificial synapses have been developed using materials commonly employed in photovoltaic devices. These materials can be synthesized with Suzuki or Stille cross-coupling polymerization [109]. They are utilized in bulk heterojunctions (BHJs), which blend donor and acceptor materials to efficiently separate electron–hole pairs at the donor–acceptor (D–A) interface due to differences in electron affinity and ionic potential, thereby enabling effective NIR light detection [110]. For instance, the BHJs of 2,2′-((2Z,2′Z)-(((4,4-bis(2-ethylhexyl)-4H-cyclopenta[2,1-b:3,4-b′]dithiophene-2,6-diyl)bis(4-(heptan-3-yloxy)thiophene-5,2-diyl))bis(methanylylidene))bis(5,6-difluoro-3-oxo-2,3-dihydro-1H-indene-2,1-diylidene))dimalononitrile (COTIC-4F)/[6,6]-phenyl-C_{71}-butyric acid methyl ester ($PC_{71}BM$)/poly[4,8-bis(5-(2-ethylhexyl)thiophen-2-yl)benzo[1,2-b;4,5-b′]dithiophene-2,6-diyl-alt-(4(2-ethylhexyl)-3-fluorothieno[3,4-b]thiophene-)-2-carboxylate2-6-diyl)] (PTB7-Th) and 2,2′-((2Z,2′Z)-(((4,4,9,9-tetrakis(4-hexylphenyl)-4,9-dihydro-sindaceno[1,2-b:5,6-b′]dithiophene-2,7-diyl)bis(4-((2-ethylhexyl)oxy)thiophene-5,2-diyl))bis(methanylylidene))bis(5,6-difluoro-3-oxo-2,3-dihydro-1H-indene-2,1-diylidene))dimalononitrile (IEICO-4F)/PTB7-Th have been used in NIR-detectable artificial synapses. COTIC-4F and IEICO-4F, which form the BHJ, serve as acceptor materials for NIR light detection [51, 60]. These materials exhibit a D–A structure, which results in a low bandgap due to intramolecular charge transfer from the electron push-pull effect between the donor and acceptor units, as shown in figure 3(e) [109, 111]. In photosensitive artificial synapses, COTIC-4F and IEICO-4F, with their A-D-A structures, demonstrate photoresponses up to 1310 nm and 980 nm, respectively. The longer wavelength detection of COTIC-4F compared to IEICO-4F is attributed to the stronger electron-donating characteristic of the core unit in COTIC-4F. This highlights that the composition of strong donor and acceptor units results in a lower bandgap [112]. Additionally, another acceptor material, 2,20-((2Z,20Z)-((12,13-bis(2ethylhexyl)-3,9-diundecyl-12,13-dihydro-[1, 2, 5]thiadiazolo[3,4-e]thieno[2,3′:4′,5′]thieno[2′,3′:4,5]pyrrolo[3,2-g]thieno[2′,3′:4,5]thieno[3,2-b]indole-2,10-diyl)bis(methanylylidene))bis(5,6-difluoro-3-oxo-2,3-dihydro-1H-indene-2,1-diylidene))dimalononitrile (Y6), which features an A-DA′D-A structure, has been reported for use in NIR-detectable artificial synapses [72]. The high planarity of the DA′D core in Y6 enhances π-delocalization, leading to bandgap reduction and enabling long-wavelength detection. Y6 exhibited light absorption at wavelengths up to 1000 nm [113]. Furthermore, single organic materials based on diketopyrrolopyrrole (DPP) and benzobisthiadiazole (BBT), both strong electron-withdrawing units, have been utilized in NIR-sensing artificial synapses [70–72, 114]. The polymer, poly[{2,5-bis-(2-octyldodecyl)-3,6-bis-(thien-2-yl)-pyrrolo[3,4-c]pyrrole-1,4-diyl}-co-{2,2′-(2,1,3-benzothiadiazole)-5,5′-diyl}] (PODTPPD-BT), synthesized with a D–A–D–A′ structure incorporating benzothiadiazole (BT) and DPP as acceptor units and two thiophenes as donor units, enhances intramolecular charge transfer and exhibits a photoresponse at the NIR wavelength of 905 nm. Additionally, the BBT-based polymer P1, with the same D–A–D–A′ structure, achieved a low bandgap of 0.69 eV and exhibited a photoresponse at wavelengths up to 1850 nm [38]. Moreover, blending acceptor and donor materials can form not only BHJs but also charge transfer complexes (CTCs), enabling NIR light detection [115–117]. Unlike BHJs, CTCs rely on strong charge transfer interactions between donor and acceptor materials, which create a low bandgap due to the hybridization and overlap of their orbitals, as illustrated in figure 3(f). Consequently, CTCs can detect NIR light even when composed of materials that individually exhibit no photoresponse in the NIR region. For example, the donor poly(3,3‴-dialkylquaterthiophene) (PQT-12) and the acceptor 2,3,5,6-tetrafluoro-7,7,8,8-tetracyanoquinodimethane (F4-TCNQ) each exhibit absorption peaks in the blue region of the visible spectrum. However, upon forming a CTC, a bandgap of 0.4 eV is created due to their strong intermolecular interactions, resulting in a wide absorption range from 350 to 3200 nm, making them promising for NIR-detectable artificial synapses [118].

3.2. Mechanism

Optoelectronic synaptic devices can emulate various synaptic properties, such as SDDP and SRDP, by mimicking synaptic structures and plasticity [119, 120]. These devices typically feature two-terminal (2T) or three-terminal (3T) structures, with the mechanisms for implementing synaptic behavior varying depending on their architecture. In 2T devices, the advantage of the simple structure is that it enables high-density integration, such as cross-bar array architectures [121–124]. However, the devices adopting random conductance modulation mechanisms may hinder the device uniformity and reliability [44, 125]. In

contrast, 3T devices have a structure that allows independent operation of the additional electrode (gate electrode) for write operations and the source/drain for read operations [126–128]. These isolated structures prevent interference between read and write operations, thereby making them advantageous for analog synaptic weight modulation and ensuring the device stability [129]. In addition, the multilayer architecture of the 3T devices provides versatile functionality, enabling their use as sensory synapses and broadening its applicability to various domains. Despite this, the structure can be complicated and suffer a larger footprint in the array compared to 2T devices [130].

In this section, we categorize the devices into 2T and 3T structures and describe their mechanisms for synaptic behavior, including electrochemical metallization (ECM), oxygen vacancies, ferroelectricity, and charge-trapping mechanisms.

3.2.1. 2-terminal devices

2T devices feature a simple structure with active layers sandwiched between two electrodes. These devices implement synaptic behavior by controlling the conductance of the active layer, which acts as the synaptic cleft between the pre-neuron (top electrode) and the post-neuron (bottom electrode). 2T devices exhibit synaptic properties such as PPF/PPD, SNDP, SRDP, and STDP by controlling conductance via ECM, modulating the concentration of oxygen vacancies, and utilizing charge trapping. Furthermore, these devices can participate in synaptic behavior mechanisms through NIR light illumination.

ECM modulates conductance by forming and breaking metallic filaments that connect the electrodes within the active layer. When voltage is applied, metal atoms in the electrode oxidize and migrate to the active layer, where they react with electrons to form metallic filaments. These filaments provide a conductive path for electron flow to the opposite electrode, switching the device from its initial high-resistance state (HRS) to a low-resistance state (LRS), resulting in an increase in current [131, 132]. The device can revert to the HRS by breaking the metallic filaments through methods such as Joule heating and ionization. NIR light can modulate conductance by assisting in the removal of metallic filaments. For example, a device with a bottom indium tin oxide (ITO) electrode, a polymethyl methacrylate (PMMA) active layer containing $MoSe_2/Bi_2Se_3$ nanosheets, and a top Ag electrode can switch from LRS to HRS under NIR illumination. At a wavelength of 790 nm, photogenerated electron–hole pairs separate, with electrons captured in the lower levels of $MoSe_2/Bi_2Se_3$ nanosheets and holes released to the PMMA. The holes strike the Ag filament, which has high electrochemical activity, causing Ag atoms to oxidize into Ag ions (figure 4(a)). As the filaments break down, the device gradually transitions from LRS to HRS, implementing synaptic depression through 790 nm NIR light [52].

Additionally, 2T devices can adjust conductance by regulating the concentration of ionized oxygen vacancies (V_o^{2+}) in the active layer. A device using oxygen-rich InGaZnO (O_R-IGZO) and oxygen-deficient InGaZnO (O_D-IGZO) as active layers utilizes this mechanism to implement synaptic properties (figure 4(b)). An interfacial barrier forms between O_D -IGZO and O_R-IGZO, and its width is influenced by the concentration of V_o^{2+}, which can be altered by illuminating O_D-IGZO with visible light. As the concentration of V_o^{2+} increases, the interfacial barrier narrows, allowing more electrons to tunnel through, thereby increasing conductance. Conversely, when NIR light illuminates O_R-IGZO, electrons in its conduction band jump or tunnel into O_D -IGZO, neutralizing V_o^{2+} to V_o. As a result, the interfacial barrier thickens and conductance decreases as the concentration of V_o^{2+} decreases. Upon removal of the light, the device exhibits gradual conductance decay as the interfacial barrier widens, demonstrating synaptic decay in photocurrent [53].

The 2T device with charge trapping can exhibit synaptic behavior by utilizing the intrinsic defect sites of the material and the potential well formed due to energy level differences between the materials. Defect sites, such as vacancies or dangling bonds at material interfaces, can capture carriers during transport. Upon light exposure, photogenerated electron–hole pairs separate, and the charges can be trapped in the material's defect sites. These trapped carriers are slowly released, preventing the current from dropping suddenly but allowing it to decay gradually. For example, a device with the structure of Au/2,2′7,7′-Tetrakis [N,N-di(4-methoxyphenyl)amino]-9,9′-spirobifluorene (Spiro-OMeTAD)/p-type Si nanocrystals:n-type $MAPbI_3$/phenyl-C_{61}-butyric acid methyl ester ($PC_{61}BM$)/ITO exhibits synaptic behavior under NIR light (figure 4(c)). Photogenerated carriers separate due to a built-in electric field between $MAPbI_3$ and Si nanocrystals, with electrons and holes moving to $PC_{61}BM$ and Spiro-OMeTAD, respectively. Some electrons are trapped in the dangling bonds of the Si nanocrystals, slowly being released, which contributes to synaptic decay. This device demonstrates various synaptic properties, including PPF, SDDP, SNDP, and SRDP under 808 nm NIR light [133]. In addition to inherent defect sites, carriers can be captured in a potential well formed by using materials with a large energy level difference. A device with an ITO/ZnO/$PC_{71}BM$/P1/MnO_3/Ag structure forms a potential well in P1. Under a negative bias, holes generated in P1 by 1550 nm light transfer to the Ag electrode due to relatively small energy level differences,

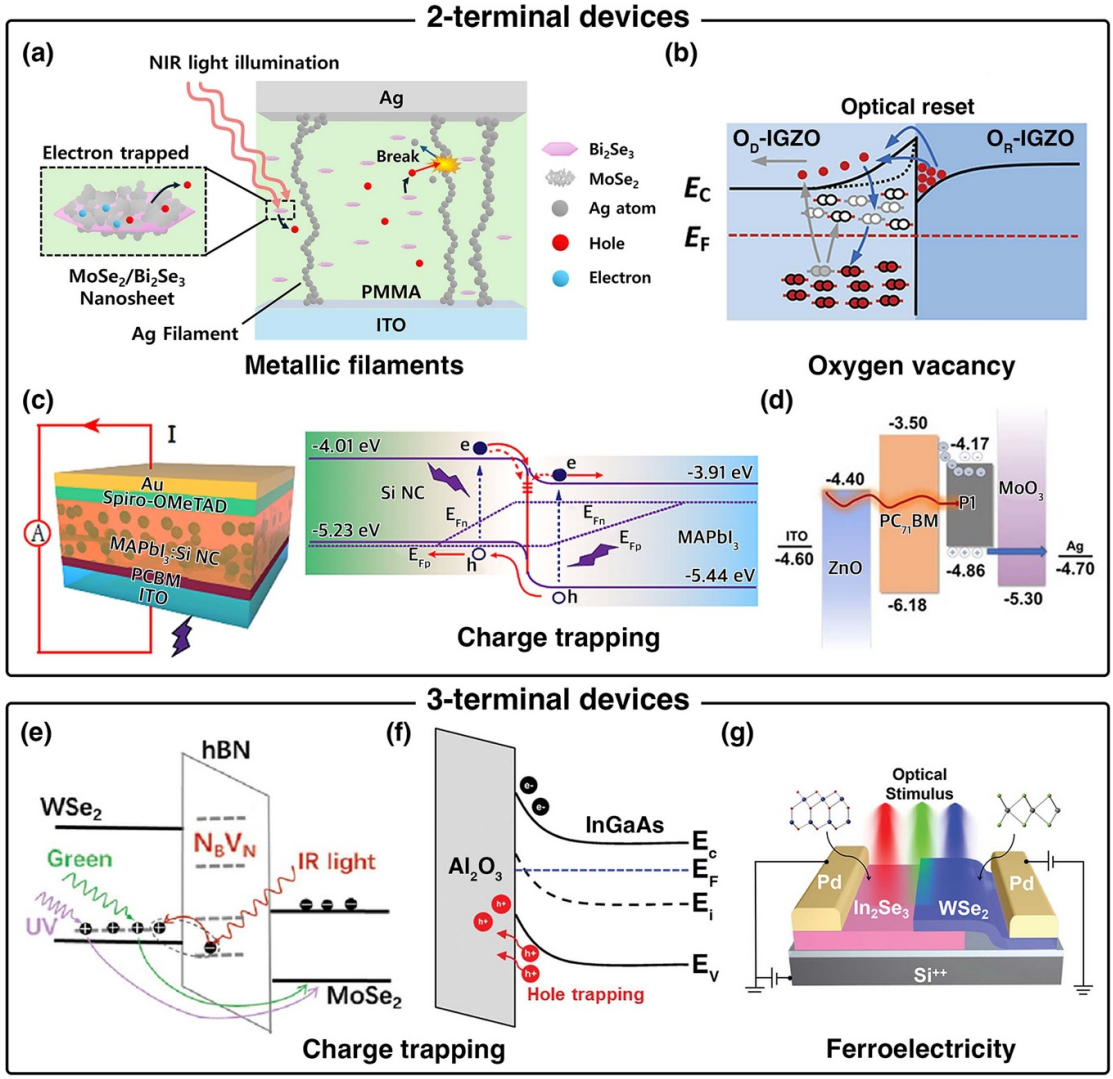

Figure 4. Various mechanisms of NIR-detectable artificial synapses. (a)–(d) 2-terminal devices: (a) metallic filaments. Disruption of metallic filaments in a memristor comprising Ag/active layer (PMMA with $MoSe_2/Bi_2Se_3$ nanosheets)/ITO under NIR light exposure [52]. (b) Oxygen vacancy. Conductance decrease process to modulate the ionized oxygen vacancy concentration in memristors using O_D-IGZO and O_R-IGZO by NIR light. Reproduced from [53]. CC BY 4.0. (c), (d) Charge trapping. (c) Potentiation process of the device of Au/Spiro-OMeTAD/p-type Si nanocrystals:n-type $MAPbI_3/PC_{61}BM$/ITO structure with NIR light to trap the photogenerated electrons. Reprinted from [133], Copyright 2020, with permission from Elsevier. (d) Displaying the synaptic behaviors with the structure of ITO/ZnO/$PC_{71}BM$/P1/MnO_3/Ag by exposure to NIR light, where photogenerated electrons are trapped in P1 by difference of the energy band difference [38]. John Wiley & Sons. © 2022 Wiley-VCH GmbH. (e)–(g) 3-terminal devices: (e), (f) Charge trapping mechanisms. (e) Synaptic decay process by removal and inducing recombination of trapped charge in WSe_2/h-BN/$MoSe_2$ structure with NIR light under negative bias [134]. John Wiley & Sons. © 2023 Wiley-VCH GmbH. (f) Hole trapping process of the device with Al_2O_3/n-type InGaAs structure with 1550 nm light under a gate bias of −0.3 V. Reproduced from [64]. CC BY 4.0. (g) Ferroelectricity. Potentiation process caused by ferroelectric polarization with NIR light of the three-terminal synaptic device with an In_2Se_3 (ferroelectric and photoresponsive) layer and a WSe_2 layer [67]. John Wiley & Sons. © 2022 Wiley-VCH GmbH.

while electrons are trapped in P1's potential well, which has larger energy level differences with $PC_{71}BM$ and MnO_3 (figure 4(d)). When the light is removed, the current decays slowly as electrons are steadily released, demonstrating synaptic decay. This device exhibits NIR-selective synaptic behaviors. Additionally, the device employing $PC_{71}BM$ showed higher PPF compared to 3,9-bis(2-methylene-(3-(1,1-dicyanomethylene)-indanone))-5,5,11,11-tetrakis(4-hexylphenyl)-dithieno[2,3-d:2′,3′-d′]-s-indaceno[1,2-b:5,6-b′]dithiophene (ITIC) and IEICO-4F due to a relatively higher lowest unoccupied molecular orbital (LUMO) energy of $PC_{71}BM$, which enhances electron trapping [38].

3.2.2. 3-terminal devices

In the 3T device structure in artificial synapse, the gate electrode acts as the presynaptic terminal that transmits the gate pulse as an action potential, while the conductance of the channel represents the synaptic weight. The conductance can be modulated by the gate pulse or light exposure, and it gradually returns to its initial state after the stimulation, exhibiting synaptic behavior. Studies investigating NIR-detectable synaptic

behaviors commonly utilize charge-trapping mechanisms, and the incorporation of ferroelectric materials has also been explored. Through these mechanisms, 3T devices exposed to NIR light exhibit various synaptic properties such as STP, LTP, and SDDP.

Charge-trapping mechanisms in 3T devices are enabled by utilizing trapping sites, such as vacancies, dangling bonds, and potential wells created by the energy level differences between materials. The trapped carriers act as an additional gate voltage that induces more carriers into the channel, increasing conductance. As the trapped carriers are gradually released after the pulse, the conductance decreases, allowing the devices to exhibit synaptic decay. For instance, a synaptic transistor employing a hexagonal boron nitride (h-BN) tunneling layer, a WSe_2 floating gate, and a $MoSe_2$ channel utilizes energy trap sites in h-BN, such as nitrogen vacancies, boron vacancies, and anti-site defects, to trap carriers (figure 4(e)). Under negative bias, holes in the channel tunnel and store in the WSe_2 floating gate layer, while electrons are trapped in the energy trap sites of h-BN. After the pulse, stored holes are gradually released to the channel by jumping through the energy trap sites of h-BN and passing through the tunneling layer, exhibiting synaptic decay. In this case, NIR light can facilitate the decay property by inducing the trapped electrons to jump to the WSe_2 floating gate, where they recombine with holes. This conductance decay mirrors synaptic behavior, making these devices promising candidates for use as synaptic devices [134].

Devices employing a pentacene channel and a MoS_2/upconversion nanoparticle floating gate, which utilize potential wells, have also been reported. Upon illumination with NIR light, upconversion nanoparticles absorb the light and re-emit at ultraviolet (UV)-visible wavelengths, generating electron–hole pairs in MoS_2. The photogenerated holes in MoS_2 drift towards pentacene, contributing to the current, while the photogenerated electrons are trapped in MoS_2. These trapped electrons act as an additional negative gate voltage, modulating the conductance of pentacene and enabling the device to exhibit multiple conductance states with increasing light intensity. Furthermore, the trapped electrons in MoS_2 can be removed by applying a large negative gate voltage of -60 V, allowing holes to move to MoS_2 and recombine with the trapped electrons. This enables the device to erase the conductance state with a large negative pulse, providing adjustability in memory states. Using this operating principle, the device can implement STP and LTP with NIR light [135].

Charge trapping can also be achieved by employing a doped extrinsic semiconductor as the channel and an insulating layer as the charge trapping layer (figure 4(f)). At the energy band alignment between the insulating layer and the n-type (or p-type) channel, minority carriers in the channel can be trapped in the insulating layer upon illumination, acting as an additional gate voltage and modulating the conductance. The trapped carriers are gradually released back into the channel and recombine with the opposite-type carriers, causing the conductance to decay. For example, a device with an n-type InGaAs channel uses an Al_2O_3 insulating layer as the charge trapping layer, trapping photogenerated holes in the Al_2O_3 layer under a gate voltage of -0.3 V. When the light is removed, the trapped holes are gradually released and recombine with electrons, exhibiting synaptic behavior through a gradual decay in photocurrent. The device demonstrated PPF and low energy consumption of 0.675 fJ under 1550 nm light with an intensity of 0.2 μW cm^{-2} [64].

By incorporating ferroelectric materials, 3T devices can implement synaptic behaviors through polarization switching. For instance, an artificial synapse using WSe_2/α-In_2Se_3 as the channel utilizes α-In_2Se_3 as both the photoresponsive and ferroelectric layer (figure 4(g)). When NIR light illuminates α-In_2Se_3 under a source-drain voltage of 0.1 V, photogenerated electron–hole pairs neutralize surface screening charges and weaken the shielding field, resulting in ferroelectric polarization switching within the domains. This switching increases the PSC. The ferroelectric polarization can switch more strongly depending on light intensity and duration, enabling the transition from STP to LTP [67, 136].

4. Applications

By integrating NIR region characteristics with artificial synapses, they can offer a vision system for environments that visible light is unable to detect and provide the opportunity to various fields that demand NIR light detection, such as health monitoring systems and military applications [137]. In addition, NIR-detectable artificial synapses allow in-sensor computing capabilities, thereby performing optical image processing within the synaptic devices themselves by constructing their own ANN, unlike conventional electronic artificial synapses which require separate sensory components [138, 139]. This allows to configurate more efficient artificial vision systems by reducing the amount of data to be processed, enabling fast processing of image information without requiring for conversion into digital data.

Due to the longer wavelength of NIR light and its reduced scattering by atmospheric particles compared to visible and UV light, it enhances image contrast, particularly in foggy and shaded areas, providing greater detail. Moreover, NIR spectral windows exhibit lower disturbances from solar irradiance than visible spectral windows. This significantly reduces ambient noise interference irrelevant to the target, enabling high

signal-to-noise ratios, thereby enhancing the operational reliability of system in outdoor [140]. This capability extends NIR night vision systems to nighttime self-driving applications, enabling recognition of moving vehicles, pedestrians, and traffic signals. Moreover, the low scattering property of NIR enables signals to travel farther, making it suitable for remote robotic control. Since NIR is invisible and does not interfere with visible-spectrum imaging, it can also support covert communication [141]. Furthermore, NIR is biocompatible and highly transmissive through biological tissues, which makes it ideal for biomedical applications, such as health monitoring and controlling artificial prostheses. Neuromorphic control systems that use NIR optical inputs provide wireless, precisely controllable, and bio-integrated solutions. These advantages highlight the unique need for NIR synaptic systems in next-generation neuromorphic vision. In this section, we discuss recent applications of NIR-detectable artificial synapses, including night vision, motion recognition systems, and robotic control systems. Moreover, we evaluate the performance of these devices in comparison to complementary metal-oxide-semiconductor (CMOS) technologies in terms of energy consumption and response time. With further progress in multispectral integration, these synapses are expected to be applied to high-level cognitive tasks such as terrain mapping and intention recognition.

4.1. Night vision and motion recognition systems

At night, only a small amount of light is reflected off objects and reaches our eyes. However, many animals have evolved photoreceptor cells that enable vision under complete darkness. Inspired by such biological systems, night vision technologies require high sensitivity and photoresponsivity to detect and recognize images in low-light conditions.

A basic image memory system capable of detecting low-intensity light has been developed [64]. A 4×4 transistor array, incorporating InGaAs as a high-sensitivity photoactive layer and channel, and Al_2O_3 as the charge-trapping dielectric layer, was fabricated. This device demonstrates synaptic properties via charge trapping and low-intensity NIR detection when stimulated with 1550 nm NIR light. The system exhibited synaptic properties even under low-light stimulation of 0.2 μW cm^{-2}. The transistor array was stimulated with 1550 nm NIR light in the shape of the letter 'A,' demonstrating image memory functions ranging from short-term to long-term memory, maintaining memory from 1 s to 60 s (figure 5(a)). Furthermore, metal wafer bonding techniques have enabled the fabrication of NIR synaptic phototransistors on flexible polyimide substrates, offering potential for wearable night vision systems.

Another essential factor in advancing night vision systems is the ability to adapt to dynamic ambient lighting conditions, from bright moonlight to complete darkness, to detect low-intensity light. At night, astronomical phenomena can drastically change the brightness of surroundings. Visual systems in animals have developed rapid adaptation responses, allowing them to maintain visual function across a wide range of light intensities. Visual systems in animals have developed rapid adaptation responses, allowing them to maintain visual function across a wide range of light intensities. When transitioning from bright to dark environments, visual cells increase their responsivity to detect faint light signals—a process known as scotopic adaptation [143]. Initially, cone cells increase their sensitivity to light, followed by a slower saturation of rod cells, which have higher maximum sensitivity and dominate vision in darkness [144]. Conversely, when transitioning from a dark to a bright environment, visual cells reduce their responsivity, a process known as photopic adaptation. Inspired by this biological mechanism, an artificial night vision system with ambient light adaptation capabilities has been developed [68]. The system emulates photopic adaptation by dynamically adjusting photosensitivity. After exposure to 200 cd m^{-2} white light, the system's current level initially rises rapidly, mimicking cone cell adaptation, and then saturates slowly, mimicking rod cell adaptation. In addition, this system memorized 'SIR' images applied via a 10-pulse NIR train at 2 Hz under dark, 200 cd m^{-2}, and 500 cd m^{-2} ambient lighting conditions (figure 5(b)). From 500 cd m^{-2} light illumination to dark conditions, the system's PPF index increased from 127% to 132%, demonstrating scotopic adaptation. Despite slight reductions in photocurrent under white ambient light, the images remained distinguishable, illustrating the system's ability to adapt to varying environmental light levels and simulate biological synaptic properties for night vision under both dark and bright conditions. Although the photocurrent values were slightly reduced under white ambient light due to changes in the system's light sensitivity—imitating photopic adaptation—the images remained distinguishable despite variations in light intensity. This demonstrates the system's ability to simulate the biological synaptic properties of the human visual system and to retain light information in response to NIR irradiation under both dark and bright nighttime conditions, showcasing strong adaptability to dynamic environmental lighting changes.

Dynamic image processing involves recognizing and memorizing images that change over time, capturing motion and temporal variations in visual data. This is particularly important for nighttime autonomous driving, where recognizing moving vehicles, pedestrians, and traffic signals is critical. However, detecting dynamic motion at night is challenging due to low illumination. NIR, with its ability to penetrate low-light environments effectively, enables motion detection even under such conditions. Traditional motion

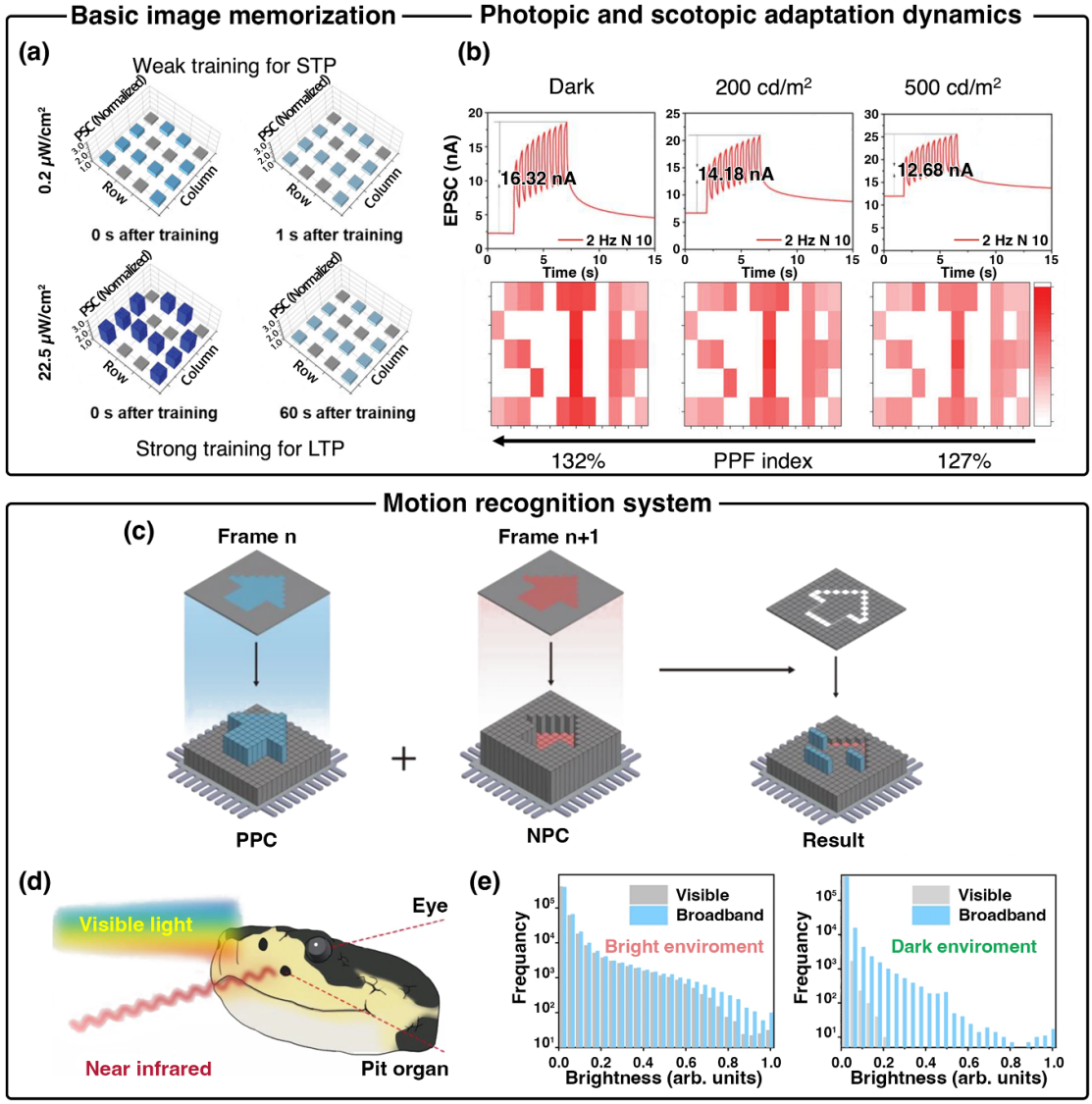

Figure 5. Applications for night vision and motion recognition systems. (a) Basic image memorization. Demonstration of short-term to long-term memory in a 4 × 4 transistor array by varying NIR light intensity from 0.2 μW cm^{-2}–22.5 μW cm^{-2}. Low-light image memory functionality is achieved through the response at 0.2 μW cm^{-2}. Reproduced from [64]. CC BY 4.0. (b) Photopic scotopic adaptation dynamics. EPSC values of the array under dark conditions, 200 cd m^{-2} white ambient light, and 500 cd m^{-2} white ambient light, along with the memorization of 'SIR' images under these varying conditions, which represents the ability to adapt to different intensities of light [68]. John Wiley & Sons. © 2022 Wiley-VCH GmbH. (c)–(e) Motion recognition systems. (c) Operation process of the MDR system: frame N is input into the PPC array, and frame $N+1$ is input into the NPC array, resulting in motion information output. (d) Biological system of snakes capable of detecting both visible and infrared radiation. (e) Brightness distribution of motion detection results in bright (left) and dark (right) environments for both visible and broadband spectra. Notably, in dark conditions, a significant enhancement of detected frequency is observed in the broadband spectrum due to the additional photoresponse from the NIR band. (c)–(e) Reproduced from [142]. CC BY 4.0.

recognition systems process information frame by frame, increasing computational and data-processing demands. By mimicking biological synapses and integrating temporal information, time-integrated data processing can significantly enhance efficiency. A motion detection and recognition (MDR) system has been developed using a bidirectional non-volatile memory function [142]. The system exhibits bipolar memory properties, characterized by positive photoconductance (PPC), which increases conductance upon light exposure, and negative photoconductance (NPC), which decreases conductance. MDR is achieved by combining arrays with opposing photoconductivity (figure 5(c)). For example, one array detects frame N using PPC, while another detects frame $N+1$ using NPC. Summing the outputs of these arrays cancels out unchanged regions, leaving only the conductance changes corresponding to motion. Inspired by the eyes and pit organs of snakes, the MDR system has been extended to operate in the NIR region. Snakes possess an ideal all-day vision system, with eyes detecting visible light and pit organs detecting NIR (figure 5(d)). Similarly, visible and NIR detection has been achieved using transistor arrays composed of transition metal dichalcogenide materials on rippled silicon nitride substrates. This broadband wavelength detection

enhances motion recognition accuracy, even at night (figure 5(e)). By efficiently sensing areas of motion, the system significantly reduces computational load and energy consumption associated with processing dynamic data. This preprocessing approach simplifies handling dynamic visual information, making the system more efficient. MDR devices capable of broadband detection, inspired by snakes' all-day vision, can improve MDR at night, including in the NIR region.

These developments suggest that NIR-detectable artificial synapses are becoming increasingly competitive with, and in some cases superior to, traditional CMOS sensors. For instance, a critical distinction lies in power consumption. Frame-based CMOS sensors tend to consume power continuously at the picojoule level, recording every pixel of every frame regardless of changes in the visual scene [145]. Optoelectronic synapses, however, operate asynchronously only when photons are incident on pixels. For example, PbS QD-based optoelectronic synapse performed power consumption as low as 0.49 fJ per event under 800 nm NIR optical pulse, showing event-driven approach can maximize power efficiency of imaging system [146]. Owing to this ultra-low energy consumption, integration of NIR-detectable artificial synapses into the system-level holds great potential of significantly higher energy efficiency compared to conventional CMOS-based imaging systems. For instance, neuromorphic imaging system based on a fully integrated optoelectronic memristor array demonstrated significantly superior energy efficiency compared to conventional graphic processing units, consuming only 94.2 nJ for low-level image preprocessing tasks and 23.9 nJ for high-level tasks like object tracking—substantially lower than the 345.8 nJ and 85.6 nJ required by graphic processing units—while maintaining comparable accuracy, with a low energy consumption of approximately 0.18 pJ per operation [146, 147]. Although it has not yet been implemented in the NIR region, the performance of this system suggests that expansion into the NIR region could be a promising strategy for advancing synapse-based imaging systems toward higher energy-efficient operation. Furthermore, NIR-detectable synaptic devices can achieve significantly lower latency and faster response times—on the order of nanoseconds for individual events—compared to conventional CMOS sensors, which typically exhibit frame readout times in the millisecond range [148–151]. For example, an artificial synapse employing an NIR-detectable InGaAs photodiode and an HfO_2 memristor demonstrated a response time of 60 ns while emulating the functions of biological retina system.

Moreover, extending optoelectronic synapses from the NIR to the visible and UV wavelength bands can combine the advantages of each spectral range. NIR can detect biological evidence such as blood flow, as its long wavelengths allow it to penetrate body tissues beneath the skin and identify bio-signals; visible light carries color information, enabling the generation of images similar to human visual perception and allowing for clear distinction between different regions; UV light can be used to identify defects on the surfaces of films or bulk materials due to its shallow penetration depth and high degrees of absorption and reflection at the material surface [152]. Combining these features enables optoelectronic synapses to be applied to terrain mapping, allowing for the differentiation of surface materials based on their spectral signatures, detection of vegetation health, and identification of water bodies or geological features—thereby creating detailed and information-rich topographical maps in both natural and urban environments, especially under challenging atmospheric or lighting conditions [153, 154]. Furthermore, it is possible to ascertain the current physiological state of the human body and to recognize behaviors and intentions. Information such as blood flow, facial expressions, and body temperature can be collected across the spectral range from visible light to the far infrared region. This approach allows for the identification of potential anomalous behavior in security-controlled areas like airports, where direct inspection is difficult due to large crowds, or for the management of patients. Recently, significant attempts had successfully integrated broadband in synaptic devices spanning from UV to infrared, demonstrating multispectral image recognition processing [155–158]. This multispectral image recognition system demonstrated effective discrimination of mixed-wavelength digit patterns, such as a digit '3' encoded in the UV spectrum superimposed upon a digit '8' in the NIR spectrum, which would otherwise be indiscernible using only single-wavelength sensing [156]. However, practical implementations of such devices in high-level tasks have yet to be realized, further progress of integrating multispectral neuromorphic vision systems with cognitive recognition system is encouraged.

4.2. Robotic control system

Utilizing NIR signals, which are invisible to the human eye, for remote control helps prevent visual distractions and avoids interference with visible light operations. This is particularly advantageous in environments such as military operations, theaters, or presentations, where visible signals could cause disruptions or reveal sensitive positions [159, 160]. Due to their high transmittance and low scattering properties, NIR optical signals enable effective communication for remote control applications [161]. For instance, remote robotic control systems utilizing NIR signals can operate in hazardous environments, deep underwater, or outer space to accomplish tasks such as rescue operations, equipment repairs, and scientific research. A robotic control system that autonomously learns using NIR optical signals has been developed to

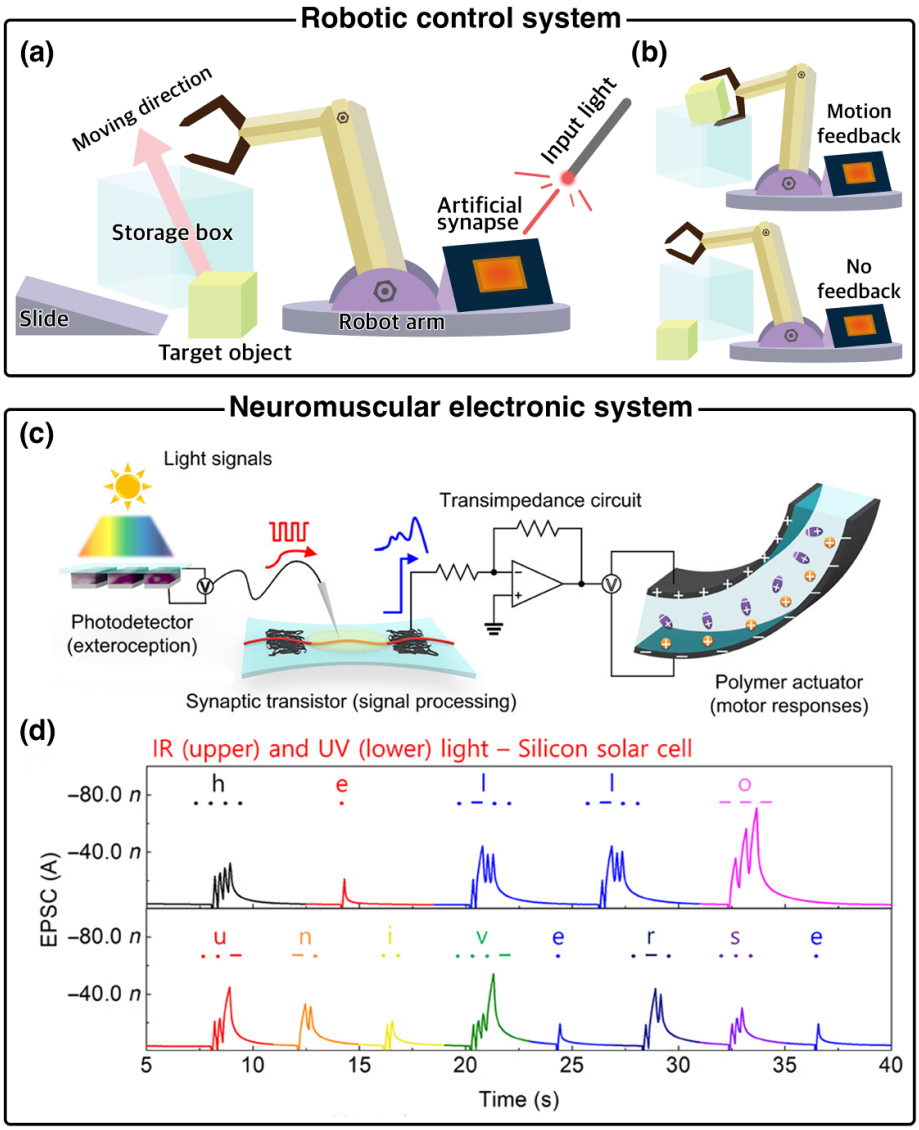

Figure 6. Applications for robotic control systems. (a), (b) Robotic control systems. Images of the optically modulated motion feedback employing an artificial synapse in a robotic control system, where repeated optical input feedback enables the action of placing an object into a storage box [162]. (c), (d) Neuromuscular electronic systems. (c) Schematic of an organic optoelectronic synapse and neuromuscular electronic system integrating a photodetector, artificial synapse, and artificial muscle actuator. (d) Organic optoelectronic system demonstrating light-triggered EPSC amplitudes across infrared to ultraviolet light, encoding the message 'hello' in International Morse code. Morse signs can be distinguished by the output current and lead to physical behavior through actuator operation. (c), (d) From [163]. Reprinted with permission from AAAS.

control robotic movements based on the synaptic weights of hydrogel-based artificial synaptic devices [162]. When a NIR pulse train is applied, ion conductivity increases, leading to an enhancement in excitatory PSC (EPSC). Once the EPSC surpasses the action potential threshold, the robot moves the target object on a slide to a storage box (figure 6(a)). During operation, after undergoing a learning phase under strong optical stimulation, the device can relearn efficiently with weaker stimulation to control the robotic hand, showing motion feedback. In contrast, systems receiving only a small optical stimulus failed to reach the re-learning process and thus failed to trigger motion feedback, that is, 'no feedback' (figure 6(b)). This highlights the simplified working process and energy efficiency enabled by relearning, mirroring the advantages of biological neuronal systems. These findings suggest that NIR could serve as a wireless communication and control medium for neuromorphic robot systems. Additionally, a neuromuscular electronic system controlled by UV-vis-NIR broadband optical signals has been proposed, bridging optoelectronic sensing with synaptic and neuromuscular control (figure 6(c)) [163]. In this system, artificial muscles are controlled through synaptic transistors, which exhibit delicate, incremental movements with low energy consumption, mimicking the behavior of biological muscles. When a light spike train stimulates a photodetector, it generates an electric spike, which is fed into a stretchable organic nanowire synaptic transistor to produce EPSC. The increased EPSC activates a polymer actuator, functioning as an artificial muscle. Additionally, as

an optical wireless communication method for human-machine interfaces, the English word 'hello' is encoded in Morse code using light pulse trains. These codes are detected by the photodetector and transmitted to the synaptic transistors, with each character distinguishable by changes in EPSC (figure 6(d)). This recognition of Morse codes demonstrates the potential for standardized communication methods in remote control applications. These results underscore the promise of NIR synaptic devices for applications in visual systems, optical communication, and robotic systems.

5. Conclusion

We have reviewed the latest advancements in NIR-detectable artificial synapses and their applications. These devices effectively mimic biological synaptic properties while detecting NIR light, enabling their use in night vision systems, dynamic motion recognition, and robotic control. Various materials, including III–V compound semiconductors, metal chalcogenides, and organic compounds, have been explored for their NIR detection capabilities. Additionally, synaptic properties have been realized through diverse device architectures and intrinsic material characteristics. In 2T memristors, mechanisms such as electrochemically conductive filaments and oxygen vacancy-based processes have been employed to achieve synaptic properties in NIR-detectable artificial synapses. In 3T transistors, synaptic functionality has been primarily enabled through charge-trapping mechanisms induced by material defects, energy band alignment, or the incorporation of ferroelectric materials. The integration of NIR photonic artificial synapses into night vision and robotic control systems offers significant advantages, including enhanced energy efficiency, improved imaging clarity, and robust remote communication capabilities due to NIR's low scattering properties.

Furthermore, introducing various materials to detect NIR light and a utilization strategy for sensitive light detection can improve the light detection performance of NIR-detectable artificial synapses. Especially, perovskite and plasmonic enhancement are practical candidates for applying to the devices. The inorganic-organic hybrid perovskites are a suitable material for employing as photoresponsive material due to their high light absorption and simple fabrication process [164]. However, they usually detect the visible region or the narrow NIR region, thus, it should be developed to reduce the bandgap. Although the composition ratio adjustment and pressure treatment for reducing their bandgap in the materials have already been studied, there are few reports on NIR-focused synaptic devices [165–168]. To enhance the photoresponse range of NIR light, plasmonic enhancement can be considered in NIR-sensing artificial synapses. When light of a frequency matching the plasmon resonance of nanoparticles is irradiated, the surface plasmon resonance effect occurs as the surface electrons oscillate collectively, enhancing light absorption as a result [169, 170]. Therefore, by expanding to the NIR-sensing artificial synapses, detecting the light with a lower intensity could be enabled, and improving the photoresponsive performance at the device level is expected.

Meanwhile, to enhance synaptic performance or implement various synaptic properties in NIR-detectable artificial synapses, phase-change material and electrochemical material can be considered. The phase-change materials can provide new operational mechanisms in an NIR-detectable artificial synapse. The switching mechanisms of amorphous and crystalline states bidirectionally depend on the optical pulse duration and the light intensity that determines the heating temperature [171]. As the phase-change mechanisms have the merits of conductance retention characteristic and fast resistance switching speed, they are expected to enable real-time processing for the artificial visual system [172, 173]. However, there is a report utilizing this mechanism in the visible region, but the implementation in NIR-detectable artificial synapses is yet to come [174]. Additionally, the use of electrolytes and electrochemically active materials in synaptic devices has been explored as a promising strategy for biomimetic applications [175, 176]. This is because their ion migration-based operating principle resembles that of biological synapses [177, 178]. When these mechanisms are integrated with NIR light detection, synaptic devices can be advanced into artificial multi-sensory systems that emulate the multimodal sensing ability of biological systems and lead to the bio-hybrid system [16]. Although some materials such as p(C2F-z), poly(benzimidazobenzophenanthroline) (BBL), and P(gNDI-gT2) have recently been reported, the search for materials with simultaneous NIR-photoresponsive and electrochemically active properties still remains attractive [57, 179].

Despite these promising advancements, several challenges remain in the practical application of NIR-detectable artificial synapses. One key limitation is resolution. While commercial NIR imaging systems for nighttime road condition recognition achieve a pixel pitch of approximately 15 μm, recent developments in high-definition image sensors have pushed this down to 5 μm [180, 181]. However, current NIR photonic synaptic devices have only achieved a pixel pitch of 156 μm [182]. To meet the stringent resolution requirements of imaging applications, advanced patterning techniques that ensure uniform and reliable device performance should be developed.

Another critical challenge is achieving high sensitivity and a high signal-to-noise ratio, which are essential for applications such as biological analysis, crop monitoring, art restoration, and other non-destructive evaluations [183, 184]. Detecting subtle differences in NIR signals, whether reflected or transmitted through various materials, is crucial. For instance, non-invasive medical applications such as biopsies require sensors capable of detecting faint NIR signals penetrating living tissues. Recent studies have demonstrated the potential of organic photodetectors for monitoring heart rate by leveraging NIR's ability to permeate biological tissue [185]. Energy consumption also remains a significant concern. The energy required to stimulate artificial synapses should be minimized to ensure overall system efficiency. In light-stimulated artificial synapses, energy consumption is determined by the light energy density, device size, and pulse duration [186, 187]. Addressing challenges related to resolution, sensitivity, and device size will directly contribute to reducing system-wide energy demands. Higher resolution enables smaller light sources for activation, while enhanced synaptic sensitivity allows devices to function with lower-intensity light sources, further lowering power consumption. If these limitations can be addressed, NIR-detectable artificial synapses hold immense potential for advanced applications in optical communication and visual data processing. Potential use cases include military-grade night vision, autonomous night driving, biological sample analysis, and remote-controlled robotic systems.

For system-level advancement, addressing cell-to-cell writing disturbance and crosstalk is critical when integrating NIR-detectable artificial synapses in large-scale arrays. In conventional electrical artificial synapses, this issue has been mitigated by incorporating access elements such as transistors, diodes, and selectors to block unintended signals from affecting unselected cells [188–193]. In contrast, optoelectronic synapses utilize light as the writing stimulus, inherently eliminating such electrical interference issues in electrical systems [194–196]. However, as device integration density increases for high-performance applications, the probability of optical writing disturbances—where unintended adjacent devices are also triggered by incident light—rises significantly. Thus, precise and localized optical stimulation becomes a critical technological requirement. To the best of our knowledge, NIR-detectable artificial synapses have not yet been demonstrated at array scales large enough, hence, initial efforts for follow-up research focusing on realizing such large-scale arrays are recommended. Furthermore, a recent study demonstrated that configuring an array with wavelength-selective photonic devices enables accurate, interference-free writing and reading of information associated with each wavelength, even under high integration density. A 28-bit optical memory system, consisting of wavelength-selective optical random-access memory (RAM) array has realized independently divided memorization and successful retrieval of multiple optical signal based on wavelength under simultaneous irradiation [197]. The light pulse signals with different wavelengths were directly guided to their corresponding optical RAMs due to the wavelength-selective nanocavities in the devices, enabling the simultaneous writing of multiple signals without writing disturbance or crosstalk. This demonstration implies the potential to implement tens of thousands of channels per square millimeter in terms of areal density, highlighting the feasibility of multi-channel, interference-free operation.

Moreover, from the perspective of utilizing NIR-detectable artificial synapses as image sensors, addressing the interconnect bottleneck is also critical. In conventional CMOS-based image sensor systems, this issue has been alleviated by directly stacking dynamic RAM (DRAM) onto image sensors using through-silicon via technology, thereby enabling high-frame-rate processing. However, this approach requires a dedicated DRAM cell for each pixel, significantly increasing manufacturing costs. In contrast, optoelectronic synapses offer in-sensor computing capabilities, allowing immediate processing of optical signals upon detection without the need for additional memory [198]. This not only overcomes cost-related limitations but also enhances system efficiency by enabling pre-image processing at the device-level, thereby reducing the volume of data transmitted to post-image processors [138].

After that, the future development directions for NIR-detectable artificial synapses are as follows. First, integrating these devices with event-based cameras expected to improve their readout speed and energy efficiency. Unlike CMOS-based image sensors in conventional cameras, which produce analog electrical signals proportional to light intensity via photodiodes, dynamic vision sensors (DVSs) in event-based cameras operate only when changes in brightness occur at each pixel, generating spike-like outputs solely in response to increases or decreases in illumination [199, 200]. However, to perform motion recognition, large volumes of spike-like output must be transmitted to processors, leading to time latency and energy consumption, which counteracts the efficiency benefits of DVS [201–204]. Since optoelectronic synapses could enable the unification of DVS and processing functionalities within a single device by allowing simultaneous generation and processing of spike signals, NIR-detectable artificial synapses represent a promising component for event-based cameras, offering faster response times, reduced energy consumption, and the combining benefit of NIR sensing [139, 200].

Although capturing images in low-light condition, adaptation to dynamic lighting conditions, and real-time image recognition and memorization—similar to those in biological vision systems—has been

demonstrated using NIR-detectable artificial synapses, other practical properties such as biocompatibility and high transmittance of NIR to biological tissues that could be applied to health monitoring and biomedical applications have not been fully exploited, and further advancements are necessary [205]. Real-time adaptive learning has garnered significant attention in fields such as education and healthcare/rehabilitation using wearable devices, as it enables dynamic adjustment of learning content based on the learner's responses and condition. When integrated with NIR sensing technology, such systems can provide quantitative, real-time feedback on the learner's physiological and cognitive states by detecting biological indicators such as cerebral blood flow, hence offering a more personalized and effective learning experience [206–208]. Therefore, the integration of NIR-detectable artificial synapses into real-time adaptive learning systems could replace conventional photodetectors and learning process units by simultaneously providing NIR sensing and adaptive learning functionalities, thereby enhancing system portability and enabling compact device architectures.

Lastly, integration of NIR-detectable synaptic devices with silicon photonics is worth noting, as it is a crucial technology for future commercialization. The compatibility of NIR-detectable artificial synapses with silicon-based technologies has already been demonstrated in several studies [50, 70, 149]. In particular, materials such as III–V semiconductors have shown compatibility with thin-film deposition methods like metal-organic chemical-vapor deposition and MBE, as well as with photolithography and etching processes, which are already well established in standard CMOS fabrication [64, 209]. However, polymer-based NIR-sensing materials are hardly compatible with commercial fabrication processes due to the following issues: (i) orthogonality problems with photoresists and their solvents or developer in photolithography processes, and (ii) thermal instability that may occur due to high temperatures (400 °C–500 °C) used during metallization steps in back-end-of-line processing [210–212]. To address these issues, one study demonstrated that the use of highly fluorinated chemicals as photoresists can achieve orthogonality with polymers, as polymers are mostly either oleophilic or hydrophilic [213]. Furthermore, in an effort to impart chemical and physical tolerance to polymer semiconductors, a recent study showed that introducing bridged polysilsesquioxanes (BPSQs) into polymer semiconductors can provide resistance to solvents used in photolithography and to mechanical degradation during etching processes. Using CMOS fabrication processes of photolithography and etching, an inverter fabricated with a polymer semiconductor incorporating a BPSQ network exhibited no noticeable degradation in its optoelectronic performance, as the BPSQ network firmly anchors the polymer chains, thereby enhancing resistance to dissolution and physical damage [214]. However, as the need for low-temperature fabrication processes remains, further research on fabrication strategies is necessary.

In summary, the development of NIR-detectable artificial synapses represents a significant step forward in bridging neuromorphic technology with NIR photodetection. These devices exhibit remarkable potential across various fields by emulating biological synaptic properties while enabling NIR detection. However, to fully realize their capabilities, further research is required to overcome challenges such as pixel pitch, sensitivity, and signal-to-noise ratio. These future advancements in device fabrication techniques and material development will be crucial for achieving high-resolution, high-sensitivity artificial synapses, ultimately expanding their range to applications, including event-based cameras, real-time adaptive learning systems, and integration with silicon photonics.

Data availability statement

No new data were created or analysed in this study.

Acknowledgment

This research was supported by Seoul National University of Science and Technology.

ORCID iDs

Minjun Choi 0009-0006-8598-2008
Gwoncheol Choi 0009-0004-8343-7968
Seungbeom Lee 0009-0000-3182-6612
Tae-Woo Lee 0000-0002-6449-6725
Hea-Lim Park 0000-0001-8370-7068

References

[1] Wang J, Geng Y-J, Guo B, Klima T, Lal B N, Willerson J T and Casscells W 2002 Near-infrared spectroscopic characterization of human advanced atherosclerotic plaques *J. Am. Coll Cardiol.* **39** 1305–13

[2] Vitorino R, Barros A S, Guedes S, Caixeta D C and Sabino-Silva R 2023 Diagnostic and monitoring applications using near infrared (NIR) spectroscopy in cancer and other diseases *Photodiagnosis Photodyn. Ther.* **42** 103633

[3] Baykal D, Irrechukwu O, Lin P C, Fritton K, Spencer R G and Pleshko N 2010 Nondestructive assessment of engineered cartilage constructs using near-infrared spectroscopy *Appl. Spectrosc.* **64** 1160–6

[4] Afara I, Prasadam I, Crawford R, Xiao Y and Oloyede A 2012 Non-destructive evaluation of articular cartilage defects using near-infrared (NIR) spectroscopy in osteoarthritic rat models and its direct relation to Mankin score *Osteoarthr. Cartil* **20** 1367–73

[5] Brown C P, Bowden J C, Rintoul L, Meder R, Oloyede A and Crawford R W 2009 Diffuse reflectance near infrared spectroscopy can distinguish normal from enzymatically digested cartilage *Phys. Med. Biol.* **54** 5579–94

[6] Kenry, Duan Y and Liu B 2018 Recent advances of optical imaging in the second near-infrared window *Adv. Mater.* **30** 1802394

[7] Chen Y, Wang S and Zhang F 2023 Near-infrared luminescence high-contrast *in vivo* biomedical imaging *Nat. Rev. Bioeng.* **1** 60–78

[8] Lim T, Bae S H, Yu S H, Baek K-Y and Cho S 2022 Near-infrared reflective dark-tone bilayer system for LiDAR-based autonomous vehicles *Macromol. Res.* **30** 342–7

[9] Luo Y, Remillard J and Hoetzer D 2010 Pedestrian detection in near-infrared night vision system *2010 IEEE Intell. Veh. Symp.* pp 51–58

[10] Yu H, Chen J, Mi R, Yang J and Liu Y-G 2021 Broadband near-infrared emission of K_3ScF_6:Cr^{3+} phosphors for night vision imaging system sources *Chem. Eng. J.* **417** 129271

[11] Hertel D, Marechal H, Tefera D A, Fan W and Hicks R 2009 A low-cost VIS-NIR true color night vision video system based on a wide dynamic range CMOS imager *2009 IEEE Intell. Veh. Symp.* pp 273–8

[12] Li Z, Pu S, Ji M, Zeng F and Li B 2024 Visible and near-infrared image fusion based on information complementarity *CAAI Trans. Intell. Technol.* **10** 1–14

[13] Huang C T, Wang Z and Kuo C-C J 2016 Visible-light and near-infrared face recognition at a distance *J. Vis. Commun. Image Represent.* **41** 140–53

[14] Zou X, Xu S, Chen X, Yan L and Han Y 2021 Breaking the von Neumann bottleneck: architecture-level processing-in-memory technology *Sci. China Inf. Sci.* **64** 160404

[15] Jung U, Kim M, Jang J, Bae J H, Kang I M and Lee S H 2024 Formation of cluster-structured metallic filaments in organic memristors for wearable neuromorphic systems with bio-mimetic synaptic weight distributions *Adv. Sci.* **11** 2307494

[16] Kim K-N, Sung M-J, Park H-L, Lee T-W, Kim K-N, Sung M-J, Lee T-W and Park H-L 2022 Organic synaptic transistors for bio-hybrid neuromorphic electronics *Adv. Electron. Mater.* **8** 2100935

[17] Huang W, Xia X, Zhu C, Steichen P, Quan W, Mao W, Yang J, Chu L and Li X 2021 Memristive artificial synapses for neuromorphic computing *Nano-Micro Lett.* **13** 85

[18] Kim H, Kim M, Lee A, Park H-L, Jang J, Bae J-H, Kang I M, Kim E-S and Lee S-H 2023 Organic memristor-based flexible neural networks with bio-realistic synaptic plasticity for complex combinatorial optimization *Adv. Sci.* **10** 2300659

[19] Park H L, Kim M-H, Kim H and Lee S-H 2021 Self-selective organic memristor by engineered conductive nanofilament diffusion for realization of practical neuromorphic system *Adv. Electron. Mater.* **7** 2100299

[20] Oh S, Kim H, Kim S E, Kim M-H, Park H-L and Lee S-H 2023 Biodegradable and flexible polymer-based memristor possessing optimized synaptic plasticity for eco-friendly wearable neural networks with high energy efficiency *Adv. Intell. Syst.* **5** 2200272

[21] Kim S E, Kim M-H, Jang J, Kim H, Kim S, Jang J, Bae J-H, Kang I M and Lee S-H 2022 Systematic engineering of metal ion injection in memristors for complex neuromorphic computing with high energy efficiency *Adv. Intell. Syst.* **4** 2200110

[22] Kim S G, Han J S, Kim H, Kim S Y and Jang H W 2018 Recent advances in memristive materials for artificial synapses *Adv. Mater. Technol.* **3** 1800457

[23] Dai S, Zhao Y, Wang Y, Zhang J, Fang L, Jin S, Shao Y and Huang J 2019 Recent advances in transistor-based artificial synapses *Adv. Funct. Mater.* **29** 1903700

[24] Choi C, Lee G J, Chang S, Song Y M and Kim D H 2024 Inspiration from visual ecology for advancing multifunctional robotic vision systems: bio-inspired electronic eyes and neuromorphic image sensors *Adv. Mater.* **36** 2412252

[25] Saarinen A, Harjunen V, Jasinskaja-Lahti I, Jääskeläinen I P and Ravaja N 2021 Social touch experience in different contexts: a review *Neurosci. Biobehav. Rev.* **131** 360–72

[26] Mu B, Guo L, Liao J, Xie P, Ding G, Lv Z, Zhou Y, Han S-T and Yan Y 2021 Near-infrared artificial synapses for artificial sensory neuron system *Small* **17** 2103837

[27] Wang J *et al* 2024 An infrared near-sensor reservoir computing system based on large-dynamic-space memristor with tens of thousands of states for dynamic gesture perception *Adv. Sci.* **11** 2307359

[28] Connors B W and Long M A 2004 Electrical synapses in the mammalian brain *Annu. Rev. Neurosci.* **27** 393–418

[29] Miller A C and Pereda A E 2017 The electrical synapse: molecular complexities at the gap and beyond *Dev. Neurobiol.* **77** 562–74

[30] Zucker R S and Regehr W G 2002 Short-term synaptic plasticity *Annu. Rev. Physiol.* **64** 355–405

[31] Voglis G and Tavernarakis N 2006 The role of synaptic ion channels in synaptic plasticity *EMBO Rep.* **7** 1104–10

[32] Mayford M, Siegelbaum S A and Kandel E R 2012 Synapses and memory storage *Cold Spring Harbor Perspect. Biol.* **4** a005751

[33] Turrigiano G G 2008 The self-tuning neuron: synaptic scaling of excitatory synapses *Cell* **135** 422–35

[34] Taube J and Schwartzkroin P 1988 Mechanisms of long-term potentiation: EPSP/spike dissociation, intradendritic recordings, and glutamate sensitivity *J. Neurosci.* **8** 1632–44

[35] Waldeck R F, Pereda A and Faber D S 2000 Properties and plasticity of paired-pulse depression at a central synapse *J. Neurosci.* **20** 5312–20

[36] Huang F, Meng K and Tang J 2007 Properties of paired-pulse firing thresholds and the relationship with paired-pulse plasticity in hippocampal CA3–CA1 synapses *Eur. J. Neurosci.* **25** 3253–63

[37] Park H, Lee Y, Kim N, Seo D, Go G and Lee T 2020 Flexible neuromorphic electronics for computing, soft robotics, and neuroprosthetics *Adv. Mater.* **32** 1903558

[38] Wang S, Chen H, Liu T, Wei Y, Yao G, Lin Q, Han X, Zhang C and Huang H 2023 Retina-inspired organic photonic synapses for selective detection of SWIR light *Angew. Chem., Int. Ed.* **62** e202213733

[39] Jeong U C, Ro J S, Park H L and Lee T W 2024 Modulating short-term and long-term plasticity of polymer-based artificial synapses for neuromorphic computing and beyond *Neuromorph. Comput. Eng.* **4** 032001

[40] Martinez J L and Derrick B E 1996 Long-term potentiation and learning *Annu. Rev. Psychol.* **47** 173–203
[41] Buchanan K A 2010 The activity requirements for spike timing-dependent plasticity in the hippocampus *Front. Synaptic Neurosci.* **2** 11
[42] Bi G and Poo M 1998 Synaptic modifications in cultured hippocampal neurons: dependence on spike timing, synaptic strength, and postsynaptic cell type *J. Neurosci.* **18** 10464–72
[43] Valtcheva S, Paillé V, Dembitskaya Y, Perez S, Gangarossa G, Fino E and Venance L 2017 Developmental control of spike-timing-dependent plasticity by tonic GABAergic signaling in striatum *Neuropharmacology* **121** 261–77
[44] Zhao Y, Lee S, Long T, Park H L and Lee T W 2025 Natural biomaterials for sustainable flexible neuromorphic devices *Biomaterials* **314** 122861
[45] Zhao Y, Jin Y, Wang X, Zhao J, Wu S, Li M, Wang J, Fan S and Li Q 2023 A high linearity and energy-efficient artificial synaptic device based on scalable synthesized MoS_2 *J. Mater. Chem. C* **11** 5616–24
[46] Zhang H *et al* 2023 A self-rectifying synaptic memristor array with ultrahigh weight potentiation linearity for a self-organizing-map neural network *Nano Lett.* **23** 3107–15
[47] Subin P S, Asha A S, Saji K J and Jayaraj M K 2021 Spike-dependent plasticity modulation in TiO_2-based synaptic device *J. Mater. Sci., Mater. Electron.* **32** 13051–61
[48] Ren Z Y, Zhu L Q, Guo Y B, Long T Y, Yu F, Xiao H and Lu H L 2020 Threshold-tunable, spike-rate-dependent plasticity originating from interfacial proton gating for pattern learning and memory *ACS Appl. Mater. Interfaces* **12** 7833–9
[49] Hou Y X *et al* 2021 Large-scale and flexible optical synapses for neuromorphic computing and integrated visible information sensing memory processing *ACS Nano* **15** 1497–508
[50] Yang H, Hu Y, Zhang X, Ding Y, Wang S, Su Z, Shuai Y and Hu P A 2024 Near-infrared optical synapses based on multilayer $MoSe_2$ moiré superlattice for artificial retina *Adv. Funct. Mater.* **34** 2308149
[51] Liu T *et al* 2022 Multifunctional organic vertical photodiodes for photo-detection and photo-synapse enabled by modulation of the interface energy barrier *Adv. Opt. Mater.* **10** 2201104
[52] Wang Y *et al* 2019 Near-infrared annihilation of conductive filaments in quasiplane $MoSe_2$ /Bi_2Se_3 nanosheets for mimicking heterosynaptic plasticity *Small* **15** 1805431
[53] Hu L, Yang J, Wang J, Cheng P, Chua L O and Zhuge F 2021 All-optically controlled memristor for optoelectronic neuromorphic computing *Adv. Funct. Mater.* **31** 2005582
[54] Yan T *et al* 2023 Near-infrared optoelectronic synapses based on a Te/α-In_2Se_3 heterojunction for neuromorphic computing *Sci. China Inf. Sci.* **66** 160404
[55] Tan F *et al* 2024 Multifunctional broadband artificial visual system using all-in-one two-dimensional optoelectronic transistors *Mater. Today* **81** 23–35
[56] Ouyang Y, Zhang C, Wang J, Guo Z, Wang Z and Dong M 2025 Gate-tunable dual-mode optoelectronic device for self-powered photodetector and optoelectronic synapse *Adv. Sci.* **12** e2416259
[57] Hidalgo Castillo T C, Shan W, Ma G, Zhao H, Wang Y, Druet V, Saleh A, Gu X and Inal S 2025 Thermal annealing for high performance and memory behavior in n-type organic electrochemical transistors *Adv. Mater.* **37** 2411214
[58] Zhang J, Guo Z, Sun T, Guo P, Liu X, Gao H, Dai S, Xiong L and Huang J 2024 Energy-efficient organic photoelectric synaptic transistors with environment-friendly $CuInSe_2$ quantum dots for broadband neuromorphic computing *SmartMat* **5** e1246
[59] Sun Y, Hu R, An C, Ma X, Zhang J and Liu J 2021 Visible to near-infrared photodetector based on $SnSe_2$/WSe_2 heterojunction with potential application in artificial visual neuron *Nanotechnology* **32** 475206
[60] Han C, Han J, He M, Han X, Wu Z, Yu H, Gou J and Wang J 2024 Photonic synaptic transistor with memory mode switching for neuromorphic visual system *Laser Photon. Rev.* **18** 2300976
[61] Wang C *et al* 2024 Strain-insensitive viscoelastic perovskite film for intrinsically stretchable neuromorphic vision-adaptive transistors *Nat. Commun.* **15** 3123
[62] Hestrin S and Korenbrot J I 1990 Activation kinetics of retinal cones and rods: response to intense flashes of light *J. Neurosci.* **10** 1967–73
[63] Zhang J *et al* 2023 Retina-inspired artificial synapses with ultraviolet to near-infrared broadband responses for energy-efficient neuromorphic visual systems *Adv. Funct. Mater.* **33** 2302885
[64] Kim T S, Jeon S H, Ko K, Ahn D H, Han J H, Choi W J and Yu K J 2023 Fast, energy-efficient InGaAs synaptic phototransistors on flexible substrate *Adv. Electron. Mater.* **9** 2300437
[65] Shen R, Jiang Y, Li Z, Tian J, Li S, Li T and Chen Q 2022 Near-infrared artificial optical synapse based on the P(VDF-TrFE)-coated inas nanowire field-effect transistor *Materials* **15** 8247
[66] Hu Y *et al* 2022 Flexible optical synapses based on In_2Se_3/MoS_2 heterojunctions for artificial vision systems in the near-infrared range *ACS Appl. Mater. Interfaces* **14** 55839–49
[67] Li X, Li S, Tang B, Liao J and Chen Q 2022 A Vis-SWIR photonic synapse with low power consumption based on WSe_2 /In_2Se_3 ferroelectric heterostructure *Adv. Electron. Mater.* **8** 2200343
[68] Huang X *et al* 2023 Short-wave infrared synaptic phototransistor with ambient light adaptability for flexible artificial night visual system *Adv. Funct. Mater.* **33** 2208836
[69] Huang X *et al* 2021 Dual-mode learning of ambipolar synaptic phototransistor based on 2D perovskite/organic heterojunction for flexible color recognizable visual system *Small* **17** 2102820
[70] Sha X, Cao Y, Meng L, Yao Z, Gao Y, Zhou N, Zhang Y, Chu P K and Li J 2022 Near-infrared photonic artificial synapses based on organic heterojunction phototransistors *Appl. Phys. Lett.* **120** 151103
[71] Chen H, Lv L, Wei Y, Liu T, Wang S, Shi Q and Huang H 2021 Self-powered flexible artificial synapse for near-infrared light detection *Cell Rep. Phys. Sci.* **2** 100507
[72] Kim N *et al* 2023 Molecular tailoring to achieve long-term plasticity in organic synaptic transistors for neuromorphic computing *Adv. Intell. Syst.* **5** 2300016
[73] Del Alamo J A 2011 Nanometre-scale electronics with III–V compound semiconductors *Nature* **479** 317–23
[74] Li Z, Allen J, Allen M, Tan H H, Jagadish C and Fu L 2020 Review on III–V semiconductor single nanowire-based room temperature infrared photodetectors *Materials* **13** 1400
[75] Sun J, Han M, Gu Y, Yang Z and Zeng H 2018 Recent advances in group iii–v nanowire infrared detectors *Adv. Opt. Mater.* **6** 1800256
[76] Ilyas N, Li D, Song Y, Zhong H, Jiang Y and Li W 2018 Low-dimensional materials and state-of-the-art architectures for infrared photodetection *Sensors* **18** 4163

[77] Zhang X, Li R, Yu Y, Dai F, Jiang R, Guo J, Hu W, Ni Z and Lu J 2024 Dark current mechanisms and suppression strategies for infrared photodetectors based on two-dimensional materials *Laser Photon. Rev.* **18** 2300936
[78] Rogalski A 2003 Infrared detectors: status and trends *Prog. Quantum Electron.* **27** 59–210
[79] Ting D Z, Soibel A, Khoshakhlagh A, Keo S A, Rafol S B, Fisher A M, Pepper B J, Luong E M, Hill C J and Gunapala S D 2019 Advances in III–V semiconductor infrared absorbers and detectors *Infrared Phys. Technol.* **97** 210–6
[80] Chen R-S, Yang T-H, Chen H-Y, Chen L-C, Chen K-H, Yang Y-J, Su C-H and Lin C-R 2009 High-gain photoconductivity in semiconducting InN nanowires *Appl. Phys. Lett.* **95** 162112
[81] Guo H-W, Hu Z, Liu Z-B and Tian J-G 2021 Stacking of 2D materials *Adv. Funct. Mater.* **31** 2007810
[82] Beretta D *et al* 2019 Thermoelectrics: from history, a window to the future *Mater. Sci. Eng. R* **138** 100501
[83] Woods-Robinson R, Han Y, Zhang H, Ablekim T, Khan I, Persson K A and Zakutayev A 2020 Wide band gap chalcogenide semiconductors *Chem. Rev.* **120** 4007–55
[84] Agarwal K, Rai H and Mondal S 2023 Quantum dots: an overview of synthesis, properties, and applications *Mater. Res. Express* **10** 062001
[85] Kim Y, Woo W J, Kim D, Lee S, Chung S M, Park J and Kim H 2021 Atomic-layer-deposition-based 2D transition metal chalcogenides: synthesis, modulation, and applications *Adv. Mater.* **33** 2005907
[86] Giri A, Park G and Jeong U 2023 Layer-structured anisotropic metal chalcogenides: recent advances in synthesis, modulation, and applications *Chem. Rev.* **123** 3329–442
[87] Magda G Z, Pető J, Dobrik G, Hwang C, Biró L P and Tapasztó L 2015 Exfoliation of large-area transition metal chalcogenide single layers *Sci. Rep.* **5** 14714
[88] Edvinsson T 2018 Optical quantum confinement and photocatalytic properties in two-, one- and zerodimensional nanostructures *R. Soc. Open. Sci.* **5** 180387
[89] Long M, Wang P, Fang H and Hu W 2019 Progress, challenges, and opportunities for 2D material based photodetectors *Adv. Funct. Mater.* **29** 1803807
[90] Wang H, Guo J, Miao J, Luo W, Gu Y, Xie R, Wang F, Zhang L, Wang P and Hu W 2022 Emerging single-photon detectors based on low-dimensional materials *Small* **18** 2103963
[91] Kershaw S V, Susha A S and Rogach A L 2013 Narrow bandgap colloidal metal chalcogenide quantum dots: synthetic methods, heterostructures, assemblies, electronic and infrared optical properties *Chem. Soc. Rev.* **42** 3033–87
[92] Xu K, Zhou W and Ning Z 2020 Integrated structure and device engineering for high performance and scalable quantum dot infrared photodetectors *Small* **16** 2103963
[93] Tian Y, Luo H, Chen M, Li C, Kershaw S V, Zhang R and Rogach A L 2023 Mercury chalcogenide colloidal quantum dots for infrared photodetection: from synthesis to device applications *Nanoscale* **15** 6476–504
[94] Yin X, Zhang C, Guo Y, Yang Y, Xing Y and Que W 2021 PbS QD-based photodetectors: future-oriented near-infrared detection technology *J. Mater. Chem. C* **9** 417–38
[95] Bukowski T J and Simmons J H 2002 Quantum dot research: current state and future prospects *Crit. Rev. Solid State Mater. Sci.* **27** 119–42
[96] Rühle S, Shalom M and Zaban A 2010 Quantum-dot-sensitized solar cells *ChemPhysChem* **11** 2290–304
[97] Mamiyev Z and Balayeva N O 2023 PbS nanostructures: a review of recent advances *Mater. Today Sustain.* **21** 100305
[98] Giansante C 2019 Enhancing light absorption by colloidal metal chalcogenide quantum dots via chalcogenol(ate) surface ligands *Nanoscale* **11** 9478–87
[99] Giansante C 2021 Surface chemistry impact on the light absorption by colloidal quantum dots *Chem. Eur. J.* **27** 14358–68
[100] Ren Z, Sun J, Li H, Mao P, Wei Y, Zhong X, Hu J, Yang S and Wang J 2017 Bilayer PbS quantum dots for high-performance photodetectors *Adv. Mater.* **29** 1702055
[101] Zheng H *et al* 2023 Strong interlayer coupling in twisted transition metal dichalcogenide moiré superlattices *Adv. Mater.* **35** 2210909
[102] Liu B, Xian L, Mu H, Zhao G, Liu Z, Rubio A and Wang Z F 2021 Higher-Order Band Topology in Twisted moiré superlattice *Phys. Rev. Lett.* **126** 066401
[103] Tang K and Qi W 2020 Moiré-pattern-tuned electronic structures of van der Waals heterostructures *Adv. Funct. Mater.* **30** 2002672
[104] Xia W, Dai L, Yu P, Tong X, Song W, Zhang G and Wang Z 2017 Recent progress in van der Waals heterojunctions *Nanoscale* **9** 4324–65
[105] Xu G, Liu D, Li S, Wu Y, Zhang Z, Wang S, Huang Z and Zhang Y 2022 Binary-ternary transition metal chalcogenides interlayer coupling in van der Waals type-II heterostructure for visible-infrared photodetector with efficient suppression dark currents *Nano Res.* **15** 2689–96
[106] Zheng Z, Zu X, Zhang Y and Zhou W 2020 Rational design of type-II nano-heterojunctions for nanoscale optoelectronics *Mater. Today Phys.* **15** 100262
[107] Rao G *et al* 2019 Two-dimensional heterostructure promoted infrared photodetection devices *InfoMat* **1** 272–88
[108] Liu Y, Elbanna A, Gao W, Pan J, Shen Z and Teng J 2022 Interlayer excitons in transition metal dichalcogenide semiconductors for 2D optoelectronics *Adv. Mater.* **34** 2107138
[109] Bundgaard E and Krebs F C 2007 Low band gap polymers for organic photovoltaics *Sol. Energy Mater. Sol. Cells* **91** 954–85
[110] Xie B, Chen Z, Ying L, Huang F and Cao Y 2020 Near-infrared organic photoelectric materials for light-harvesting systems: organic photovoltaics and organic photodiodes *InfoMat* **2** 57–91
[111] Dou L, Liu Y, Hong Z, Li G and Yang Y 2015 Low-bandgap near-IR conjugated polymers/molecules for organic electronics *Chem. Rev.* **115** 12633–65
[112] Meng D, Zheng R, Zhao Y, Zhang E, Dou L and Yang Y 2022 Near-infrared materials: the turning point of organic photovoltaics *Adv. Mater.* **34** 2107330
[113] Yuan J *et al* 2019 Enabling low voltage losses and high photocurrent in fullerene-free organic photovoltaics *Nat. Commun.* **10** 570
[114] Kim T, Lee W, Kim S, Lim D C and Kim Y 2024 Near-infrared-sensing flexible organic synaptic transistors with water-processable charge-trapping polymers for potential neuromorphic computing/skin applications *Adv. Intell. Syst.* **6** 2300651
[115] Goetz K P, Vermeulen D, Payne M E, Kloc C, McNeil L E and Jurchescu O D 2014 Charge-transfer complexes: new perspectives on an old class of compounds *J. Mater. Chem. C* **2** 3065–76
[116] Baharfar M, Hillier A C and Mao G 2024 Charge-transfer complexes: fundamentals and advances in catalysis, sensing, and optoelectronic applications *Adv. Mater.* **36** 2406083
[117] Wang C, Zhang X and Hu W 2020 Organic photodiodes and phototransistors toward infrared detection: materials, devices, and applications *Chem. Soc. Rev.* **49** 653–70

[118] Yang B et al 2021 High performance ternary organic phototransistors with photoresponse up to 2600 nm at room temperature *Adv. Funct. Mater.* **31** 2103787
[119] Lee H S, Ro J S, Ko G M and Park H L 2023 Flexible and stretchable synaptic devices for wearable neuromorphic electronics *Flex Print Electron.* **8** 043001
[120] Ro J S, An H M and Park H L 2023 Electrolyte-gated synaptic transistors for brain-inspired computing *Jpn. J. Appl. Phys.* **62** SE0801
[121] Li H et al 2021 Memristive crossbar arrays for storage and computing applications *Adv. Intell. Syst.* **3** 2100017
[122] Park H L, Kang S, Suh J H, Lee S D and Lee S H 2021 Balance of surface energy difference between wetting and dewetting regions for patterning solution-processed organic light-emitting diode *Org. Electron.* **95** 106203
[123] Jung U, Beak C J, Kim K, Na J H and Lee S H 2024 Scalable photo-responsive physical unclonable functions via particle kinetics *ACS Nano* **18** 27642–53
[124] Park M W, Kim D Y, An U, Jang J, Bae J H, Kang I M and Lee S H 2022 Organizing reliable polymer electrode lines in flexible neural networks via coffee ring-free micromolding in capillaries *ACS Appl. Mater. Interfaces* **14** 46819–26
[125] Seok H, Lee D, Son S, Choi H, Kim G and Kim T 2024 Beyond von Neumann architecture: brain-inspired artificial neuromorphic devices and integrated computing *Adv. Electron. Mater.* **10** 2300839
[126] An H M et al 2023 Engineered current path of vertical organic phototransistors for smart optoelectronic applications *J. Mater. Chem. C* **11** 14580–8
[127] Park H L, Jun J, Kim M H and Lee S H 2022 Introduction of helical photonic crystal insulator in organic phototransistor for enhancing selective color absorption *Org. Electron.* **100** 106385
[128] Choi J H, Hwang H S, Jang H B, Kim S U and Park H L 2024 Flexible phototransistors integrated with chiral liquid crystal encapsulating film for improving color selectivity and stability *ACS Appl. Electron. Mater.* **6** 8103
[129] Chen K and Chen J 2022 Perspective on oxide-based three-terminal artificial synapses in physical neural networks *Appl. Phys. Lett.* **121** 190501
[130] Cui J, Liu H and Cao Q 2024 Prospects and challenges of electrochemical random-access memory for deep-learning accelerators *Curr. Opin Solid State Mater. Sci.* **32** 101187
[131] Beak C J, Lee J, Kim J, Park J and Lee S-H 2024 Filamentary-based organic memristors for wearable neuromorphic computing systems *Neuromorph. Comput. Eng.* **4** 022001
[132] Kim H, Lee J, Kim H W, Woo J, Kim M-H and Lee S-H 2023 Definition of a localized conducting path via suppressed charge injection in oxide memristors for stable practical hardware neural networks *ACS Appl. Mater. Interfaces* **15** 51444–52
[133] Huang W et al 2020 Zero-power optoelectronic synaptic devices *Nano Energy* **73** 104790
[134] Xu B et al 2024 Gap state-modulated van der Waals short-term memory with broad band negative photoconductance *Small* **20** 2309626
[135] Zhai Y, Zhou Y, Yang X, Wang F, Ye W, Zhu X, She D, Lu W D and Han S-T 2020 Near infrared neuromorphic computing via upconversion-mediated optogenetics *Nano Energy* **67** 104262
[136] Chen J, You D, Zhang Y, Zhang T, Yao C, Zhang Q, Li M, Lu Y and He Y 2020 Highly sensitive and tunable self-powered UV photodetectors driven jointly by p-n junction and ferroelectric polarization *ACS Appl. Mater. Interfaces* **12** 53957–65
[137] Gundepudi K, Neelamraju P M, Sangaraju S, Dalapati G K, Ball W B, Ghosh S and Chakrabortty S 2023 A review on the role of nanotechnology in the development of near-infrared photodetectors: materials, performance metrics, and potential applications *J. Mater. Sci.* **58** 13889–924
[138] Zhang Z, Wang S, Liu C, Xie R, Hu W and Zhou P 2022 All-in-one two-dimensional retinomorphic hardware device for motion detection and recognition *Nat. Nanotechnol.* **17** 27–32
[139] Zhou Y et al 2023 Computational event-driven vision sensors for in-sensor spiking neural networks *Nat. Electron.* **13** 870–8
[140] Gates D M 1966 Spectral distribution of solar radiation at the earth's surface *Science* **151** 523–9
[141] Guri M, Hasson O, Kedma G and Elovici Y 2016 An optical covert-channel to leak data through an air-gap *2016 14th Annual Conf. on Privacy, Security and Trust (PST)* pp 642–9
[142] Pang X et al 2024 Non-volatile rippled-assisted optoelectronic array for all-day motion detection and recognition *Nat. Commun.* **15** 1613
[143] Uddin D, Jeffrey B G, Flynn O, Wong W, Wiley H, Keenan T, Chew E and Cukras C 2020 Repeatability of scotopic sensitivity and dark adaptation using a medmont dark-adapted chromatic perimeter in age-related macular degeneration *Transl. Vis. Sci. Technol.* **9** 31
[144] Kono M, Goletz P W and Crouch R K 2008 11-cis- and all-trans-retinols can activate rod opsin: rational design of the visual cycle *Biochemistry* **47** 7567–71
[145] Song H, Oh S, Salinas J, Park S Y and Yoon E 2021 A 5.1ms low-latency face detection imager with in-memory charge-domain computing of machine-learning classifiers *2021 Symp. on VLSI Circuits* pp 1–2
[146] Feng T, Xu H, Yang Y, Hu X, Wang T, Zhu H, Sun Q, Zhang D W, Meng J and Chen L 2025 Organic synaptic transistors based on C8-BTBT/PMMA/PbS QDs for UV to NIR face recognition systems *Nano Lett.* **25** 3637–45
[147] Schowitz P, Sinha S and Gujarati A 2024 Response-time analysis of a soft real-time NVIDIA holoscan application *2024 IEEE Real-Time Systems Symp. (RTSS)* pp 57–69
[148] Zhai Y, Yang X, Wang F, Li Z, Ding G, Qiu Z, Wang Y, Zhou Y and Han S-T 2018 Infrared-sensitive memory based on direct-grown MoS_2–upconversion-nanoparticle heterostructure *Adv. Mater.* **30** 1803563
[149] Bae B, Park M, Lee D, Sim I and Lee K 2023 Hetero-integrated InGaAs photodiode and oxide memristor-based artificial optical nerve for in-sensor NIR image processing *Adv. Opt. Mater.* **11** 2201905
[150] Chang S et al 2022 SWIR imaging using PbS QD photodiode array sensors *Opt. Express* **30** 20659–65
[151] Liao F, Zhou F and Chai Y 2021 Neuromorphic vision sensors: principle, progress and perspectives *J. Semicond.* **42** 013105
[152] Zhu J, Liu J, Xu T, Yuan S, Zhang Z, Jiang H, Gu H, Zhou R and Liu S 2022 Optical wafer defect inspection at the 10 nm technology node and beyond *Int. J. Extrem. Manuf.* **4** 032001
[153] Mulder V, de Bruin S, Schaepman M and Mayr T 2011 The use of remote sensing in soil and terrain mapping—A review *Geoderma* **162** 1–19
[154] Olson C F, Matthies L H, Wright J R, Li R and Di K 2007 Visual terrain mapping for Mars exploration *Comput. Vis. Image Underst.* **105** 73–85
[155] Jiang L, Yang L, Yuan Y, Zhu Q, Wu W, Wang X, Xu W and Qiu L 2024 Flexible optoelectronic synapses based on conjugated polymer blends for ultra broadband spectrum light perception *ACS Mater. Lett.* **6** 1606–15

[156] Islam M M et al 2022 Multiwavelength optoelectronic synapse with 2D materials for mixed-color pattern recognition ACS Nano 16 10188–98
[157] Li Z, Zou G, Xiao Y, Feng B, Huo J, Peng J, Sun T and Liu L 2024 MoS_2/ZnO-heterostructured optoelectronic synapse for multiwavelength optical information-based sensing, memory, and processing Nano Energy 127 109733
[158] Ni Y, Feng J, Liu J, Yu H, Wei H, Du Y, Liu L, Sun L, Zhou J and Xu W 2022 An artificial nerve capable of UV-Perception, NIR-Vis switchable plasticity modulation, and motion state monitoring Adv. Sci. 9 2102036
[159] Li Y, Wang J, Guo J, Fu C, Huang L, Chen L, Ni Y and Zheng Q 2023 UV and IR dual light triggered cellulose-based invisible actuators with high sensitivity Int. J. Biol. Macromol. 238 124031
[160] Guri M and Bykhovsky D 2019 aIR-Jumper: covert air-gap exfiltration/infiltration via security cameras & infrared (IR) Comput. Secur. 82 15–29
[161] Luo P, Sun D, Lyu Z, Wei S, Lu Z, Zhou L, Zhang X, Shen S and You H 2024 Remote control and noninvasive detection enabled by a high-performance NIR pc-LED Inorg. Chem. 63 2655–62
[162] Tian H, Wang C, Chen Y, Zheng L, Jing H, Xu L, Wang X, Liu Y and Hao J 2023 Optically modulated ionic conductivity in a hydrogel for emulating synaptic functions Sci. Adv. 9 eadd6950
[163] Lee Y et al 2018 Stretchable organic optoelectronic sensorimotor synapse Sci. Adv. 4 eaat7387
[164] Zuo C, Bolink H J, Han H, Huang J, Cahen D and Ding L 2016 Advances in perovskite solar cells Adv. Sci. 3 1500324
[165] Miah M H, Khandaker M U, Rahman M B, Nur-E-Alam M and Islam M A 2024 Band gap tuning of perovskite solar cells for enhancing the efficiency and stability: issues and prospects RSC Adv. 14 15876–906
[166] Duan J, Liu Z, Zhang Y, Liu K, He T, Wang F, Dai J and Zhou P 2018 Planar perovskite $FA_xMA_{1-x}PbI_3$ solar cell by two-step deposition method in air ambient Opt. Mater. 85 55–60
[167] Lü X, Yang W, Jia Q and Xu H 2017 Pressure-induced dramatic changes in organic-inorganic halide perovskites Chem. Sci. 8 6764–76
[168] Zhang L, Zeng Q and Wang K 2017 Pressure-induced structural and optical properties of inorganic halide perovskite $CsPbBr_3$ J. Phys. Chem. Lett. 8 3752–8
[169] Sun L, Qu S and Xu W 2023 A retinomorphic neuron for artificial vision and iris accommodation Mater. Horiz. 10 5753–62
[170] Qian X, Zhang F, Li X, Li J, Sun H, Wang Q, Huang C, Zhang Z, Zhou Z and Liu J 2025 Artificial self-powered and self-healable neuromorphic vision skin utilizing silver nanoparticle-doped ionogel photosynaptic heterostructure J. Semicond. 46 012602
[171] Raoux S, Wełnic W and Ielmini D 2010 Phase change materials and their application to nonvolatile memories Chem. Rev. 110 240–67
[172] Jeyasingh R, Fong S W, Lee J, Li Z, Chang K W, Mantegazza D, Asheghi M, Goodson K E and Wong H S 2014 Ultrafast characterization of phase-change material crystallization properties in the melt-quenched amorphous phase Nano Lett. 14 3419–26
[173] Kuzum D, Jeyasingh R G, Lee B and Wong H S 2012 Nanoelectronic programmable synapses based on phase change materials for brain-inspired computing Nano Lett. 12 2179–86
[174] Zhao P, Yan S, Xing R, Yao J, Ge X, Li K, Cheng X and Miao X 2025 Homogeneous photoelectric reservoir computing system based on chalcogenide phase change materials Mater. Today Nano 29 100576
[175] Bhunia R, Boahen E K, Kim D J, Oh H, Kong Z and Kim D H 2023 Neural-inspired artificial synapses based on low-voltage operated organic electrochemical transistors J. Mater. Chem. C 11 7485–509
[176] Huang F, Sun X, Shi Y and Pan L 2025 Flexible ionic-gel synapse devices and their applications in neuromorphic system FlexMat 2 30–54
[177] Huang M, Schwacke M, Onen M, Del Alamo J, Li J and Yildiz B 2023 Electrochemical ionic synapses: progress and perspectives Adv. Mater. 35 2205169
[178] Zhou B, Liu W, Xu Y, Jin C, Yang J and Sun J 2022 Organic electrochemical transistors toward synaptic electronics J. Appl. Phys. 55 304006
[179] Wang Y et al 2025 An optoelectrochemical synapse based on a single-component n-type mixed conductor Nat. Commun. 16 1615
[180] Manda S et al 2019 High-definition visible-SWIR InGaAs image sensor using Cu-Cu bonding of III–V to silicon wafer 2019 IEEE Int. Electron Devices Meeting (IEDM) pp 16.7.1–4
[181] Pejovic V, Georgitzikis E, Lee J, Lieberman I, Cheyns D, Heremans P and Malinowski P E 2022 Infrared colloidal quantum dot image sensors IEEE Trans. Electron Devices 69 2840–50
[182] Li D et al 2024 An active-matrix synaptic phototransistor array for in-sensor spectral processing Adv. Sci. 11 2406401
[183] Yu B, Yuan J, Yan C, Xu J, Ma C and Dai H 2023 Impact of spectral resolution and signal-to-noise ratio in Vis–NIR spectrometry on soil organic matter estimation Remote Sens. 15 4623
[184] Delaney J K, Trumpy G, Didier M, Ricciardi P and Dooley K A 2017 A high sensitivity, low noise and high spatial resolution multi-band infrared reflectography camera for the study of paintings and works on paper Herit Sci. 5 1–14
[185] Huang J et al 2020 A High-performance solution-processed organic photodetector for near-infrared sensing Adv. Mater. 32 1906027
[186] Liu D, Shi Q, Dai S, Huang J, Liu D, Shi Q, Dai S and Huang J 2020 The design of 3D-interface architecture in an ultralow-power, electrospun single-fiber synaptic transistor for neuromorphic computing Small 16 1907472
[187] Tan H et al 2018 Broadband optoelectronic synaptic devices based on silicon nanocrystals for neuromorphic computing Nano Energy 52 422–30
[188] Liu H, Lv H, Yang B, Xu X, Liu R, Liu Q, Long S and Liu M 2014 Uniformity improvement in 1T1R RRAM with gate voltage ramp programming IEEE Electron Device Lett. 35 1224–6
[189] Lv H, Xu X, Liu H, Liu R, Liu Q, Banerjee W, Sun H, Long S, Li L and Liu M 2015 Evolution of conductive filament and its impact on reliability issues in oxide-electrolyte based resistive random access memory Sci. Rep. 5 7764
[190] Hsieh M-C, Liao Y-C, Chin Y-W, Lien C-H, Chang T-S, Chih Y-D, Natarajan S, Tsai M-J, King Y-C and Lin C J 2013 Ultra high density 3D via RRAM in pure 28nm CMOS process 2013 IEEE Int. Electron Devices Meeting (IEDM) pp 10.3.1–4
[191] Yoon J, Ji Y, Lee S, Hyon J and Tour J M 2018 Low-temperature-processed SiO_x one diode–one resistor crossbar array and its flexible memory application Adv. Electron. Mater. 4 1700665
[192] Wang Z et al 2018 Threshold switching of Ag or Cu in dielectrics: materials, mechanism, and applications Adv. Funct. Mater. 28 1802159
[193] Zhao X et al 2018 Breaking the current-retention dilemma in cation-based resistive switching devices utilizing graphene with controlled defects Adv. Mater. 30 1705193
[194] Zhu C et al 2022 Optical synaptic devices with ultra-low power consumption for neuromorphic computing Light Sci. Appl. 11 337

[195] Zhou M, Zhao Y, Gu X, Zhang Q, Zhang J, Jiang M and Lu S 2023 Light-stimulated low-power artificial synapse based on a single GaN nanowire for neuromorphic computing *Photon. Res.* **11** 1667
[196] Liu J *et al* 2021 Weak light-stimulated synaptic hybrid phototransistors based on islandlike perovskite films prepared by spin coating *ACS Appl. Mater. Interfaces* **13** 13362–71
[197] Kuramochi E, Nozaki K, Shinya A, Takeda K, Sato T, Matsuo S, Taniyama H, Sumikura H and Notomi M 2014 Large-scale integration of wavelength-addressable all-optical memories on a photonic crystal chip *Nat. Photon.* **8** 474–81
[198] Chen J, Zhou Z, Kim B J, Zhou Y, Wang Z, Wan T, Yan J, Kang J, Ahn J-H and Chai Y 2023 Optoelectronic graded neurons for bioinspired in-sensor motion perception *Nat. Nanotechnol.* **18** 882–8
[199] El Gamal A and Eltoukhy H 2005 CMOS image sensors *IEEE Circuits Devices Mag.* **21** 6–20
[200] Lichtsteiner P, Posch C and Delbruck T 2008 A 128×128 120 dB 15 μs latency asynchronous temporal contrast vision sensor *IEEE J. Solid-State Circuits* **43** 566–76
[201] Davies M *et al* 2018 Loihi: a neuromorphic manycore processor with on-chip learning *IEEE Micro* **38** 82–99
[202] Gallego G *et al* 2022 Event-based vision: a survey *IEEE Trans. Pattern Anal. Mach. Intell.* **44** 154–80
[203] Chen G, Cao H, Conradt J, Tang H, Rohrbein F and Knoll A 2020 Event-based neuromorphic vision for autonomous driving: a paradigm shift for bio-inspired visual sensing and perception *IEEE Signal Process. Mag.* **37** 34–49
[204] Bing Z, Meschede C, Chen G, Knoll A and Huang K 2020 Indirect and direct training of spiking neural networks for end-to-end control of a lane-keeping vehicle *Neural Netw.* **121** 21–36
[205] Shapley R and Enroth-Cugell C 1984 *Visual Adaptation and Retinal Gain Controls* (Progress in Retinal Research) ch 9 (https://doi.org/10.1016/0278-4327(84)90011-7)
[206] Karmakar S, Kamilya S, Dey P, Guhathakurta P K, Dalui M, Bera T K, Halder S, Koley C, Pal T and Basu A 2023 Real time detection of cognitive load using fNIRS: a deep learning approach *Biomed. Signal Process. Control* **80** 104227
[207] Cho S, Chang W K, Park J, Lee S H, Lee J, Han C E, Paik N-J and Kim W-S 2022 Feasibility study of immersive virtual prism adaptation therapy with depth-sensing camera using functional near-infrared spectroscopy in healthy adults *Sci. Rep.* **12** 767
[208] Abdelnour A F and Huppert T 2009 Real-time imaging of human brain function by near-infrared spectroscopy using an adaptive general linear model *Neuroimage* **46** 133–43
[209] Choi D, Harris J S, Kim E, McIntyre P C, Cagnon J and Stemmer S 2009 High-quality III–V semiconductor MBE growth on Ge/Si virtual substrates for metal-oxide-semiconductor device fabrication *J. Cryst. Growth* **311** 1962–71
[210] Malinowski P E *et al* 2014 Photolithographic patterning of organic photodetectors with a non-fluorinated photoresist system *Org. Electron.* **15** 2355–9
[211] Chrissafis K and Bikiaris D 2011 Can nanoparticles really enhance thermal stability of polymers? Part I: an overview on thermal decomposition of addition polymers *Thermochim. Acta* **523** 1–24
[212] Batude P *et al* 2011 Advances, challenges and opportunities in 3D CMOS sequential integration *2011 IEEE Int. Electron Devices Meeting (IEDM)* pp 7.3.1–4
[213] Zakhidov A A, Lee J-K, DeFranco J A, Fong H H, Taylor P G, Chatzichristidi M, Ober C K and Malliaras G G 2011 Orthogonal processing: a new strategy for organic electronics *Chem. Sci.* **2** 1178
[214] Park H W *et al* 2019 Universal route to impart orthogonality to polymer semiconductors for sub-micrometer tandem electronics *Adv. Mater.* **31** 1901400